Modeling and optimization of a photocatalytic process: Degradation of endocrine disruptor compounds by Ag/ZnO

Alma Berenice Jasso-Salcedo, Sandrine Hoppe, Fernand Pla, Vladimir Alonso Escobar-Barrios, Mauricio Camargo, Dimitrios Meimaroglou

Modeling and optimization of a photocatalytic process: Degradation of endocrine disruptor compounds by Ag/ZnO

Alma Berenice Jasso-Salcedo[a1], Sandrine Hoppe[b], Fernand Pla[b], Vladimir Alonso Escobar-Barrios[c], Mauricio Camargo[d] and Dimitrios Meimaroglou[b*]

[a]Instituto Potosino de Investigación Científica y Tecnológica, División Ciencias Ambientales, Camino a la Presa de San José 2055, Col. Lomas 4a Sección. C.P. 78216, San Luis Potosí, S.L.P., México.

[b]CNRS, Laboratoire Réactions et Génie des Procédés, Université de Lorraine UMR 7274, Nancy, F-54001, France.

[c]Instituto Potosino de Investigación Científica y Tecnológica, División de Materiales Avanzados, Camino a la Presa de San José 2055, Col. Lomas 4a Sección. C.P. 78216, San Luis Potosí, S.L.P., México.

[d]Université de Lorraine, ERPI, Equipe de Recherche sur les Processus Innovatifs, EA 6737, Nancy, F-54001, France.

*Corresponding author e-mail address: dimitrios.meimaroglou@univ-lorraine.fr

[1] Present address author AB Jasso-Salcedo: Department of Materials and Environmental Chemistry, Arrhenius Laboratory, Stockholm University, SE-106 91 Stockholm, Sweden.

Keywords: artificial neural networks, optimization, photocatalysis, bisphenol-A.

Abstract

Artificial neural network (ANN) modeling was applied to study the photocatalytic degradation of bisphenol-A. The operating conditions of the Ag/ZnO photocatalyst synthesis and its performance were simultaneously modeled and subsequently optimized to target the highest efficiency in terms of the degradation reaction rate. Two ANN models were developed to simulate the stages of the photocatalyst synthesis and photodegradation performance,

respectively. A direct dependence between the two networks was also established, thus making it possible to directly relate the degradation rate of the contaminant, not only to the photodegradation conditions, but also to the photocatalyst synthesis conditions. In this respect, an optimization study was carried out, by means of an evolutionary algorithm, in order to identify the optimal synthesis and photodegradation conditions that would result in the degradation of a maximal amount of the contaminant. Through this integrated approach it was demonstrated that neural network models can be proven valuable tools in the evaluation, simulation and, ultimately, the optimization of different stages of complex photocatalytic processes towards the maximization of the efficiency of the synthesized photocatalyst.

1 Introduction

Endocrine-disrupting compounds (EDCs) is a class of chemical substances that pollute water and other environmental resources. They are responsible for adverse developmental, reproductive, neurological and immune side-effects on both humans and wildlife as they interfere with the organism's endocrine system. Bisphenol-A (BPA) is an EDC that was used initially (i.e., in the 1930's) as an estrogenic drug for birth control and later as a monomer in the synthesis of polycarbonate as well as an additive in the synthesis of polyvinylchloride, polyesters, epoxy resins, lacquer coatings, etc. It is these latter applications that have facilitated the extensive, worldwide spread of this contaminant, presently detected in various aqueous media including fresh and marine surface waters and groundwater (Flint et al., 2012; Klečka et al., 2009).

Among the several studies on the removal of EDCs and pharmaceuticals from drinking water, sunlight-induced photocatalytic degradation is an attractive approach that has gained significant attention over the last years (Bohdziewicz et al., 2016; Esplugas et al., 2007; Fernández et al., 2014; Sin et al., 2012; Sornalingam et al., 2016; Tijani et al., 2013). Yet, despite the undisputed advantages of the process, such as its clean – non-chemical nature and its relatively low cost, heterogeneous photocatalysis is a complex process whose efficiency is related to a number of factors associated with the catalyst properties (e.g., crystal structure, morphology, surface area, defect sites, polarity, active surface sites and reactive charges life-time) and the photocatalytic reaction conditions (e.g., pH, contaminant concentration, catalyst dose, light intensity). Hence, the control of the photocatalytic performance of UV/Metal Oxide systems is not a trivial problem since it requires an optimal combination of the above

mentioned material and process characteristics and conditions. In this respect, the development of an accurate robust mathematical model of the process becomes of profound importance to the study and implementation of this decontamination technique.

Traditional modeling approaches of such systems are based on kinetic models that simulate the contaminant degradation curves on the basis of a commonly adopted first-order kinetics equation (Amani-Ghadim & Seyed Dorraji, 2015; Rosenfeldt & Linden, 2004; R. Wang et al., 2009). On the other hand, alternative modeling methodologies (e.g., empirical models or response surface methodologies) (Asl et al., 2012; Babaei et al., 2011; Kiattisaksiri et al., 2015; Lee & Hamid, 2015; Merabet et al., 2016) are constantly gaining ground in the area, mainly due to the complex nature of the photodegradation processes and the lack of thorough understanding of all the mechanisms involved, which inhibits the development of generalized powerful mechanistic models. Among these alternatives, Artificial Neural Network models display an evergrowing presence in the most recent relevant studies.

Artificial Neural Networks (ANN) are powerful tools that can be implemented on a set of raw experimental data to establish non-linear mathematical relations between the input/output of the process. They belong to the general class of ‘data-driven models’ (DDM), which attempt to create connections between the input variables and the responses of a system, without requiring any prior knowledge on the underlying physical phenomena (Solomatine et al., 2008). Other advantages of this class of models are their ability to extract and recognize patterns in data, as well as their rather quick and simple development and implementation to completely different processes.

Under the condition of existence of a sufficient number of experimental data, ANN models can be proven quite efficient and accurate, both in correlating the existing data as well as in predicting the system behavior (within the limits of the explored experimental space), while they can also be easily customized to different systems. They are commonly developed with the aid of specifically designed software or software package toolboxes (e.g., the ANN toolbox of Matlab®), which are simple to use and quite flexible in terms of the customization of the model structure and characteristics (Sivanandam et al., 2006).

A review of the implementation of ANN on heterogeneous photocatalytic water and wastewater treatment processes was published by Khataee and Kasiri (2010). The accuracy of ANN models was also assessed in a recent study by Amani-Ghadim and Seyed Dorraji (2015), who compared three different model types, namely a kinetic model, an empirical model and an ANN model on the photodegradation of Acid blue 9 using UV/ZnO. In this study, the authors investigated the effect of different factors (i.e., contaminant initial concentration, ZnO content, light intensity, pH and time) on the photodegradation efficiency and concluded that ANN modeling allows an accurate description of the photocatalytic process without the necessity to resort to complex mathematical descriptions of the kinetics.

Traditionally, ANN models have been applied to photocatalytic degradation processes in order to study the effect of a variety of reaction conditions on the photocatalytic performance by means of percentage of degradation or removal efficiency. It is only recently that the apparent reaction rate constant of a first-order photocatalytic degradation curve was considered as the simulated response of the developed ANN model (Behnajady & Eskandarloo, 2015; Delnavaz, 2015). The characteristics of a series of similar recent studies are summarized in Table 1.

As can be seen, ANN models can be used to assess the effect of numerous important factors of the process, such as light intensity, organic/inorganic ions concentration and oxygen dose, which influence the photocatalytic performance but are rarely considered in kinetic models. For instance, Vaez et al. (2015) studied the effect of anions naturally present in wastewater (i.e., sulfate SO_4^{2-}, chloride Cl^-, bicarbonate HCO_3^- and carbonate CO_3^{2-}) and peroxide, on the photodegradation of Acid Red 73 on UV/TiO_2 nanoparticles immobilized on sackcloth fiber. In another noteworthy example, Tanasa et al. (2013) successfully studied the effect of both photocatalyst properties (i.e., crystallite size, surface area and absorption edge) and reaction conditions (i.e., dye initial concentration, time and catalyst dose) on the color removal of Eosin Y in UV/ZnO/SnO_2 systems.

In the present work, a novel modeling framework is proposed for the study of a photocatalytic degradation process of a water contaminant. In this respect, the two major stages of the photocatalytic process, namely the photocatalyst synthesis and the contaminant degradation experiments, are decoupled in order to separately assess the effects of the factors affecting these two process stages on the overall photocatalytic efficiency of the synthesized photocatalyst. Two artificial neural networks are developed for the modeling of these two stages, linked together by the fact that the output of the ANN model on the photocatalyst synthesis is, at the same time, an input for the ANN model on the photodegradation experiments. In a subsequent optimization analysis, the two models are separately optimized in the inverse order (i.e., starting from the model on the photodegradation tests), thus connecting the photodegradation efficiency (i.e., related to the objective function of the first optimization

121 study on the second ANN model) with the photocatalyst synthesis conditions (i.e., optimal
122 decision variables of the second optimization study on the first ANN model).
123 The system under study concerns the use of silver-modified ZnO particles (Ag/ZnO) as effective
124 catalysts for the photodegradation of BPA in water. ZnO, charged with silver nanoparticles
125 (AgNPs), is a prominent photocatalyst that has been employed in several contaminant
126 photodegradation studies due to its decreased charge-carriers recombination rate, increased
127 photostability and efficiency (Georgekutty et al., 2008; J. Wang et al., 2011; Xie et al., 2010).
128 The detailed characteristics of the experimental system have been extensively presented in a
129 recent publication (Jasso-Salcedo et al., 2016) and will not be the subject of the present work.
130 To the best of the authors' knowledge, this is the first time that a two-stage, de-coupled ANN
131 modelling framework is proposed for the study and, subsequently, the optimization of the
132 photocatalytic degradation of an endocrine disrupting contaminant. The proposed approach
133 allows for the evaluation of the effects of the factors of the two principal stages of the
134 photodegradation process (i.e., the catalyst synthesis and the degradation experiments) on the
135 final photodegradation efficiency, by distinguishing these two stages without completely
136 isolating them from the overall process.
137

138

139 **Table 1.** Neural Network modeling studies of the photocatalytic performance on the degradation of water contaminants.

Photocatalyst	Model contaminant	ANN Topology (In:Hid:Out)	Data number	Input / Factors	Output / Response	Reference
ZnO	Acid Blue 9	5:9:1	152	AB9, pH, ZnO, UV intensity	Degradation efficiency (%)	Amani-Ghadim and Seyed Dorraji (2015)
ZnO/Montmorillonite K10	Disperse Red 54 (DR54)	5:10:1	N/A	DR54, ZnO/MMT, time	Decolorization efficiency (%)	Kiransan et al. (2015)
ZnO/Montmorillonite K10	Basic yellow 28 (BY28)	3:14:1	N/A	BY28, ZnO/MMT dosage, UV radiation time	Decolorization efficiency (%)	Kıransan et al. (2015)
TiO_2	Acid Red 27	4:8:1	56	TiO_2, AR27, pH, UV intensity	Reaction rate constant (Kap)	Behnajady and Eskandarloo (2015)
TiO_2-Light expanded clay aggregates	Phenol	5:6:4:2	325	Reaction time, Phenol, pH, TiO_2, UV intensity	Photocatalytic reactor efficiency (%) and Kinetic constant (Kapp)	Delnavaz (2015)
TiO_2/sackcloth fibre	Acid Red 73	5: 15:1	300	pH, time, anion, H_2O_2, AR73 concentration	Photocatalytic efficiency (%)	Vaez et al. (2015)
SnO_2/Fe_3O_4	Phenol red	4:20:30:20:1	30	SnO_2/Fe_3O_4, phenol red, stirring intensity, UV intensity	Dye removal (%)	Sargolzaei et al 2015
TiO_2/ZrO_2	Carbamazepine (CBZ)	4:5:1	130	TiO_2/ZrO_2, pH, reaction time, CBZ	CBZ removal (%)	Das et al. (2014)
TiO_2	Chromium (Cr (VI)	4:4:1	558	Cr(VI), pH, TiO_2, irradiation time	Photocatalytic reduction Cr (VI) (%)	Sabonian and Behnajady (2014)
TiO_2	N,N-diethyl-m-toluamide (DEET)	3:13:1	17	TiO_2, DEET, UV intensity	Photocatalytic oxidation (%)	Antonopoulou and Konstantinou (2013)
TiO_2	Total phenolic compounds (TPh)	3:12:1	17	TiO_2, TPh, UV intensity	Photocatalytic oxidation of TPh (%)	Antonopoulou et al. (2012)
TiO_2	17α-ethynylestradiol (EE2)	5:13:1	222	Reaction time, TiO_2, EE2, water dissolved organic carbon, water conductivity	EE2 conversion (%)	Frontistis et al. (2012)
TiO_2	4-nitrophenol (4-NP)	4:14:1	147	Nano TiO_2 , time, UV intensity, 4-NP	Removal (%)	Ghanbary et al. (2012)
TiO2	Reactive black 5 (RB5)	4:10:1	N/A	pH, TiO_2 dose, RB5, time	Photocatalytic efficiency (%)	Dutta et al. (2010)

140

2 Methodology

2.1 Data collection

2.1.1 Preparation of Ag/ZnO

The Ag/ZnO photocatalyst was prepared by photodeposition (PD) and impregnation (IMP) methods (Jasso-Salcedo et al., 2014). For both methods, a suspension containing ZnO and stabilized silver nanoparticles (AgNPs) was adjusted at desired initial pH values using 0.1N HCl and/or 0.5 N NaOH. The suspension was stirred under UV irradiation or in darkness, for PD and IMP methods, respectively. Then the sample was submitted to centrifugation/re-dispersion cycles in distilled water and ethanol solutions several times to remove the free AgNPs (i.e., not attached to the ZnO surface). The actual weight percentage of AgNPs that were finally attached to the ZnO surface was calculated by the following expression:

$$W_{\mathrm{Ag}}\% = \frac{W_{\mathrm{Ag}}}{W_{\mathrm{Ag}}+W_{\mathrm{Zn}}}\ 100 \quad (1)$$

where the quantities of Ag and Zn were obtained from elemental quantification using inductively coupled plasma spectrometry (ICP-OES, 730-ES, Varian Inc.) at 328 nm and 213.9 nm, respectively. Before the analysis, the samples were submitted to acid digestion (69% Nitric acid), diluted with DI H2O and filtered (0.45 um).

2.1.2 Photocatalysis experiments

An aqueous solution of BPA and photocatalyst was mechanically stirred for 10 min in darkness and then irradiated at different wavelengths, namely at 254, 302 or 365 nm using a UV lamp (3UV-38, UVP Inc.) and at 450 nm using a fluorescent lamp (F8T5/CW, Hampton Bay). The

experiments were carried out in a dark box, with the lamp placed at a distance of 8 cm above the sample, at room temperature and without external oxygen supply (Jasso-Salcedo et al., 2014). Samples were then collected at regular time intervals and centrifuged at 3,000 rpm for 10 min to recover the photocatalyst powder. The liquid samples were filtered (0.45 μm) before liquid chromatography (HPLC 1200 Series, Agilent Technologies) analysis.

The apparent kinetic rate constant of the BPA degradation was obtained as follows: the experimental data (i.e, BPA concentration vs time plots) were initially approximated by an exponential decay function, as shown in Eq.(2):

$$C_N = a\exp(bt)\,;\quad b < 0 \tag{2}$$

where C_N denotes the normalized BPA concentration (C/C_0). A least squares regression provided the values of α and b for each experiment. In order to associate the BPA degradation curves with a rate constant, the differential form of Eq.(2) was then transformed into a typical rate function of order n:

$$r\left(=-\frac{dC_N}{dt}\right)=k_{app}{C_N}^n \tag{3}$$

In the above equation, k_{app} and n are the apparent kinetic rate constant and the order of the reaction, respectively and r denotes the rate of the reaction. The values of k_{app} and n can be estimated by substituting Eq.(2) into Eq.(3):

$$\begin{cases} n=1 \\ k_{app}=-b \end{cases}$$

The first order rate of the BPA degradation was also confirmed by plotting *ln(r) vs ln(C_N)* and estimating the regression parameters of the produced straight line, according to the linearized form of Eq.(3):

$$\ln(r) = \ln(k_{app}) + n\ln(C_N) \quad (4)$$

Note that the value of the correlation coefficient, *R*, of this linear regression is given, for each experiment, in Table 5, along with the values of the experimental measurements.

2.2 Artificial neural network modeling

A neural network is a cluster of processing nodes (i.e., neurons) arranged in several layers and interconnected in a variety of topologies, following the paradigm of the functionality of the human brain. The successful development and implementation of an ANN model relies onto three principal conditions, each one with its own significance for the accuracy and efficiency of the developed model:

I. Correct identification of the input and output variables of the system, also called factors and responses, respectively. The selection of the principal factors (i.e., the ones with the greatest effect on the targeted response) from all possible candidates is a procedure that requires a minimum knowledge of the actual process. Its importance lies in the fact that the number and nature of the selected factors will affect, on the one hand, the number of required experimental data (i.e., the more factors considered, the greater the number of data required for an accurate model development), and on the other hand, will define whether important effects on the measured response have been omitted. In the case where prior knowledge on the process is completely absent, a small number of exploratory experiments can be carried out.

II. Definition of the experimental space and execution of a set of experiments for the acquisition of data. Given that the main factors of the process have been correctly

identified and under the assumption that there exists a correlation between these factors and the targeted response of the system, an ANN model can identify this correlation on the basis of a set of experimental data. Evidently, the ability of the ANN to successfully correlate the input(s) (i.e., factors) and output(s) (i.e., response(s)) is directly proportional to the number of available data. On the other hand, the number of experiments that can be carried out is always subject to feasibility constraints (e.g., time and/or cost limitations, etc.) that may dictate the studied process. Hence, the implementation of an experimental design strategy can become invaluable during this second stage of the model development procedure. The Design of Experiments (DoE) approach enables to obtain a maximum amount of information from a given predefined experimental effort. Typical DoE strategies include full- or fractional-factorial designs, central composite designs, Box–Behnken designs , Plackett– Burman (PB) designs, D-optimal and E-optimal designs, etc. (Ferreira et al., 2007; Georgakis, 2013; Heiligers, 1994; Witek-Krowiak et al., 2014).

III. Identification of the topology of the ANN: The structure of the network, in terms of the number and size of the hidden layers, as well as its characteristics (i.e., training algorithm, type of transfer functions, etc.), display a significant effect on the accuracy of the model. To identify these parameters, most studies follow a trial and error procedure where different topologies of the ANN are tested until satisfactory accuracy has been achieved. Note that the random initialization of the values of the network parameters (e.g., the neuron's weights) as well as of the data separation (c.f. next paragraph) must be taken into account during this procedure.

225 Once the experimental data have been acquired and the factors/responses and architecture of
226 the ANN model have been defined, the development of the model proceeds via a series of
227 subsequent training (i.e., parametric identification) steps. In general, the accuracy of such
228 models is assessed in terms of different statistical magnitudes, such as the Mean Square Error,
229 MSE, or the correlation coefficient, R, calculated on the basis of the comparison of the model
230 responses and the respective experimental targets. These latter are divided into three distinct
231 subsets that serve for the training, validation and testing of the network, respectively. The
232 training data set is used for the identification of the model parameters while the test data set is
233 used to assess the accuracy of the model on a set of data different than the ones used for the
234 training and validation processes. The validation data set is used to avoid overfitting
235 phenomena by monitoring the error (i.e., on this data set) throughout the training process. This
236 error normally decreases along with the training set error. An increase on the validation error
237 for a number of sequential epochs (i.e., training *passes* of the network) is an indication of
238 overfitting that triggers the stopping of the training process, returning the network (i.e., the
239 values of weights and biases) corresponding to the minimum value of the validation error. In
240 the present work, the number of sequential epochs of increasing validation error before
241 stopping the training of the network was set to seven.
242 Among the various types of existing ANNs, the most commonly encountered in physicochemical
243 process modeling is the feed-forward (i.e., the responses of each layer are used as inputs of the
244 next layer) back-propagation (i.e., the measured error at the output layer is back transferred to
245 re-adjust the model parameter values) network, while the sigmoidal (e.g., logarithmic sigmoidal
246 or tangent hyperbolic sigmoidal) and linear transfer functions are widely applied on the hidden

247 and output layers, respectively (Cheng & Titterington, 1994; Haykin, 1994; Meireles et al., 2003;
248 Sivanandam et al., 2006). Additional details on the principles and the characteristics of neural
249 networks can be found in the relevant literature (Cheng & Titterington, 1994; Haykin, 1994;
250 Meireles et al., 2003; Sivanandam et al., 2006).
251 Photocatalytic processes are greatly influenced by both catalyst properties and reaction
252 conditions. These effects are traditionally studied separately (see Table 1), probably due to the
253 complexity of assessing them simultaneously in a single study. An exception to this rule is the
254 work of Tanasa et al. (2013), who studied the system of Eosin Y dye photocatalytic degradation
255 using ZnO/SnO_2, taking into account the effects of crystallite size, surface area, absorption
256 edge, catalyst dose and total organic carbon values in their model that was developed on the
257 basis of a set of 547 experimental data. In addition, another commonly adopted practice is the
258 consideration of the irradiation time as a factor in the modeling of the percentage of
259 contaminant degradation (i.e., response). Given that the percentage of contaminant
260 degradation will normally increase with the reaction time, this approach finally leads to a rather
261 obvious correlation that, in turn, may come in the cost of missing other important effects of
262 different factors.
263 In the present work, a model development is presented that does not comply with the above
264 commonly adopted approaches. In order to combine the effects of both important stages of the
265 photocatalytic process, namely the catalyst synthesis and the photodegradation experiments, a
266 two-stage decoupled ANN model is developed where the response of the first network
267 becomes a factor for the second network. Thus, in the first stage of the model, the effects of
268 three operating conditions of the synthesis of Ag/ZnO (i.e., nominal silver concentration, pH

and reaction time, which were identified in Jasso-Salcedo et al., 2014 as the most significant parameters of the process) on the actual amount of Ag attached on the surface of ZnO of the synthesized photocatalyst were assessed in terms of an initial neural network, henceforth called ANN_1. In the second stage of this modelling framework, the effect of the actual amount of Ag attached on the surface of ZnO, pH of the medium, initial contaminant concentration and wavelength of light on the photodegradation performance of the photocatalyst were assessed in terms of a second neural network, ANN_2. A direct dependence between the two networks was established by directly introducing the response of ANN_1 as a factor of ANN_2. The photodegradation performance (i.e., the response of ANN_2) was evaluated in terms of an apparent kinetic rate constant, k_{app}, of the degradation reaction of BPA. This way, the photocatalyst synthesis conditions were directly associated to its final photodegradation performance, taking simultaneously into account the effects of the photodegradation conditions. Note that, since the evaluation of the performance of the photocatalyst was based on the rate of degradation of the contaminant, there was no need to consider the irradiation time among the factors of the photodegradation process, which was kept constant for all experiments and equal to 120 min.

The experimental ranges of all factors of the two sub-models (i.e., ANN_1 and ANN_2) are given in Tables 2 and 3, respectively. Note that for the modification experiments of ZnO, a central composite design was employed. The photocatalyst concentration used for the degradation tests was set to 1 g/L. A general schematic of the proposed modeling framework is shown in Scheme 1.

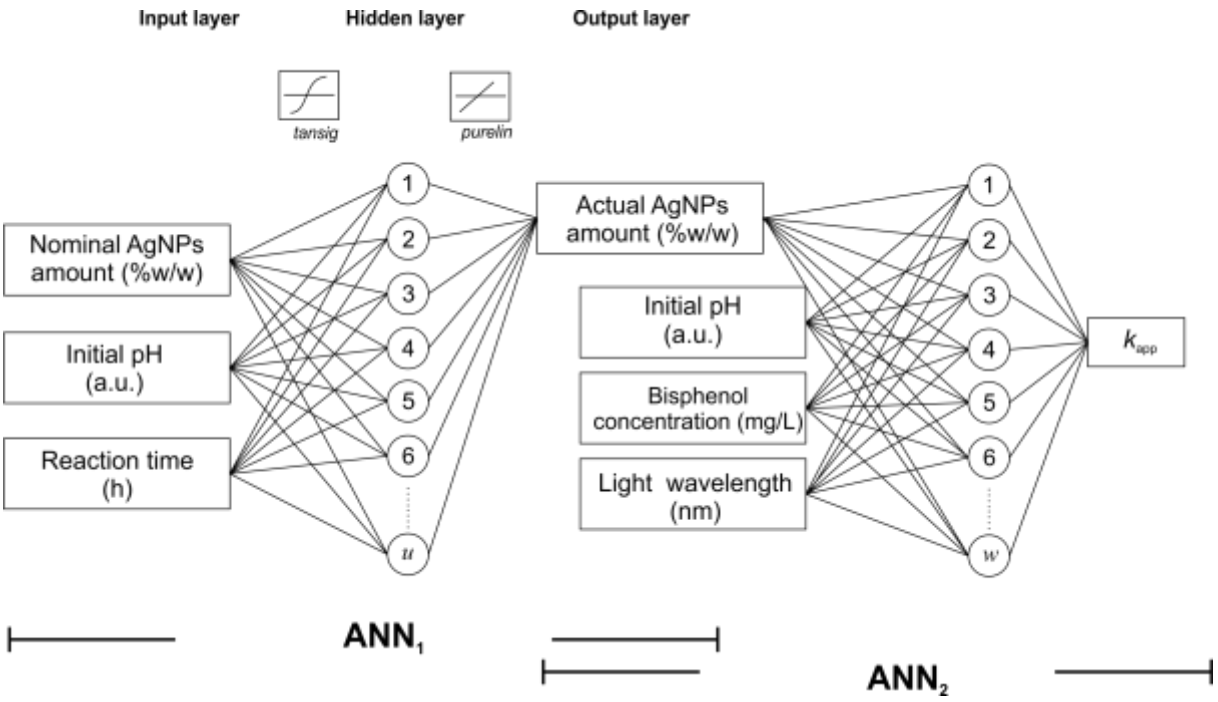

Scheme 1. Description of the input/output characteristics and connecting points of the two ANN models.

Table 2. Experimental range of the Ag/ZnO photocatalyst synthesis conditions

Input variables	**Photodeposition**	**Impregnation**
Nominal amount AgNPs (% w/w)	0.1-1	0.1-5
Initial pH	7-11	7-11
Time (h)	0.5-1	2-5

Table 3. Experimental range of the photodegradation test conditions

Input variables	
Initial pH	2.8 to 10.5
Actual amount AgNPs (%w/w)	0-1.2
Bisphenol-A (mg/L)	10-40
Wavelength (nm)	254, 302, 365 and 450

2.2.1 Neural network structure

A multi-layer feedforward network with Levenberg-Marquardt learning algorithm was used in this study. The experimental data corresponding to each model were randomly divided into training, validation and testing subsets (50 %, 25 % and 25 % of data, respectively). All data were normalized in the range [-1:1] prior to their introduction into the models.

The topology of the network models, denoted as (In:Hid:Out), corresponds to the numbers of neurons in the input, hidden and output layers, respectively. Several configurations of the network were tested to determine the best number of neurons in the hidden layer(s), based on the values of the MSE of the data sets. The MSE value between the ANN model predictions and the experimental data is typically calculated by the expression:

$$MSE = \frac{\sum_{j=1}^{N}\left(y_j^{\mathrm{mod}} - y_j^{\mathrm{exp}}\right)^2}{N} \quad (5)$$

where the exponents 'mod' and 'exp' denote the outputs of the model (i.e., the responses) and the experiment (i.e., the targets), respectively and N is the total number of experimental data. Note that, in the present work, log-sigmoidal and linear transfer functions were used for hidden and output layers, respectively. The Neural Network Toolbox of the commercial software package MATLAB 8.3.0.532 (academic license) was used for the development of the models.

2.3 Optimization study

An ultimate purpose of process models, especially data-driven models, is their implementation in an optimization study in order to identify the combination of the different process conditions that will result to the desired properties/performance of the product/process under study. Among the plethora of different mathematical methods and techniques that have been

developed for the treatment of optimization problems, evolutionary algorithms constitute a powerful approach with specific advantages and disadvantages.

In general, an evolutionary algorithm (EA) is based on the principle of the continuous improvement of a criterion (i.e., the optimization criterion) of the individuals of a population. The initial population is composed of a large set of randomly selected individuals (e.g. experimental conditions), which are characterized by a measured property or model response (e.g., the degradation efficiency corresponding to each of these experiments). The population is classified from the best individual to the worst, according to its corresponding value of the criterion and depending on whether the problem is a minimization or a maximization one, and is subsequently subjected to a series of cycles of improvement of this criterion. The best individuals are combined to generate new ones that might perform better, while the worst individuals are removed from the population after each cycle and the procedure continues until the population has "evolved" to such a point where the desired convergence to an optimal has been achieved. Detailed information on the theoretical basis of EAs for mono- and multi-objective optimization, applied on physicochemical processes, can be found in the relevant literature (Camargo et al., 2011; Fonteix et al., 1995; Viennet et al., 1996; Xi et al., 2013). EAs have also been successfully implemented in the optimization study of the degradation of phenol by a combined photocatalysis/electro-Fenton system (Khataee et al., 2014).

In the present work, an optimization study, on the basis of an EA, was also carried out in order to identify the optimal catalyst synthesis and photodegradation conditions that would result to the highest photodegradation rate of BPA. In accordance to the two-stage structure of the model, the optimization was also carried out in two consecutive steps, following an *inverse*

direction. In this respect, an initial optimization problem was solved on the basis of ANN_2 in order to identify the different photodegradation conditions that would result to a maximum degradation rate of BPA. Among these conditions, the pH, BPA concentration and light wavelength can be directly set to their optimized values, according to the results of this first optimization study. On the other hand, the actual silver content of the photocatalyst depends on the conditions of the photocatalyst synthesis process. Hence, a second optimization problem was subsequently solved, via the implementation of an EA on the basis of ANN_1, in order to identify the photocatalyst synthesis conditions that would result in the optimal amount of attached AgNPs on the ZnO surface, as defined by the output of the first optimization run. Thus, both important stages of the overall process (i.e., the synthesis of the photocatalyst and its subsequent use in the photodegradation experiments) were taken into account and their optimal conditions were identified in view of a maximal photodegradation rate of BPA. The overall optimization approach is schematically depicted in Scheme 2.

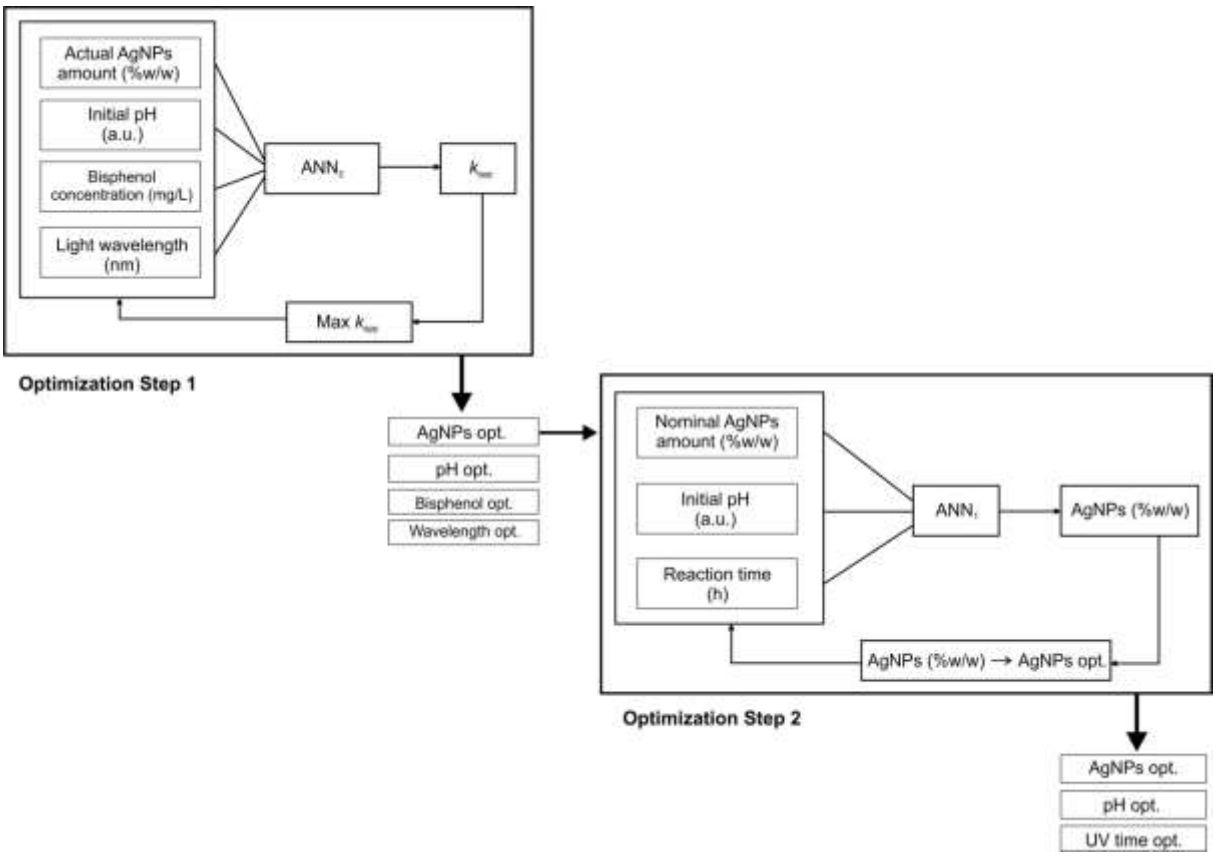

354

355 **Scheme 2.** Methodology used on the Evolutionary Algorithm - ANN coupled optimization approach on this study.

356

357 ## 3 Results and discussion

358 The development of the two ANN sub-models was based on a total of 63 experiments for ANN_1
359 and 27 experiments for ANN_2, divided into the two methods of the photocatalyst synthesis (i.e.,
360 PD and IMP methods) as shown in Tables 4 and 5. On the basis of these experimental data, the
361 identification of the optimal network topologies initially took place and subsequently the ANN
362 models were tested and validated before their implementation into the optimization study.

363

364

365 **Table 4.** Experimental conditions for the synthesis of Ag/ZnO photocatalyst and actual amount of Ag attached to the ZnO surface as measured
366 experimentally and predicted theoretically by the ANN_1 models

Nominal Ag %w/w	pH	Reaction time (min)	Attached Ag %w/w (experimental)	Attached Ag %w/w (ANN_1 model)	Nominal Ag %w/w	pH	Reaction time (min)	Attached Ag %w/w (experimental)	Attached Ag %w/w (ANN_1 model)
Photodeposition method					**Impregnation method**				
0.3573	7	30	0.320	0.327	0.1072	7	60	0.100	0.116
0.3573	7	60	0.342	0.348	0.1072	7	120	0.106	0.121
0.1073	7	30	0.082	0.084	0.1072	7	300	0.094	0.094
0.1073	7	60	0.107	0.102	1.0623	7	60	1.179	1.179
1.0623	7	30	0.991	0.920	1.0623	7	120	1.203	1.203
1.0623	7	60	1.093	1.099	1.0623	7	300	0.820	0.807
0.3573	9	30	0.358	0.356	5.095	7	60	0.521	0.522
0.3573	9	60	0.375	0.378	5.095	7	120	0.585	0.773
0.1073	9	30	0.062	0.062	5.095	7	300	0.668	0.671
0.1073	9	60	0.074	0.075	0.1072	9	60	0.099	0.093
1.0623	9	30	1.170	1.104	0.1072	9	120	0.110	0.110
1.0623	9	60	1.132	1.130	0.1072	9	300	0.096	0.100
0.3573	11	30	0.454	0.451	1.0623	9	60	0.970	1.012
0.3573	11	60	0.426	0.397	1.0623	9	120	1.192	1.188
0.1073	11	30	0.091	0.092	1.0623	9	300	1.194	1.193
0.1073	11	60	0.116	0.121	5.095	9	60	0.423	1.044
1.0623	11	30	1.183	1.182	5.095	9	120	0.494	0.336
1.0623	11	60	1.147	1.137	5.095	9	300	0.571	0.580
0.3573	7	45	0.320	0.325	0.1072	11	60	0.116	0.105
0.1073	9	45	0.074	0.071	0.1072	11	120	0.121	0.121
1.0623	9	45	1.132	1.132	0.1072	11	300	0.116	0.120
0.3573	9	45	0.362	0.365	1.0623	11	60	0.239	0.239
0.1073	7	45	0.096	0.096	1.0623	11	120	0.366	0.561
0.1073	11	45	0.103	0.102	1.0623	11	300	1.108	1.101
1.0623	7	45	1.050	1.054	5.095	11	60	0.374	0.375

1.0623	11	45	1.162	1.161	5.095	11	120	0.389	1.144
0.3573	9	45	0.371	0.365	5.095	11	300	0.498	0.503
0.3573	9	45	0.368	0.365	1.0623	9	120	1.169	1.188
0.3573	9	45	0.385	0.365	1.0623	9	120	1.223	1.188
0.3573	9	45	0.357	0.365	1.0623	9	120	1.023	1.188
0.3573	9	45	0.362	0.365	1.0623	9	120	1.179	1.188
					1.0623	9	120	1.167	1.188

367

368

369 ### 3.1 Selection of optimal network topology

370 The selection of the network topology was based on a typical trial and error approach where the number of neurons of the hidden
371 layer(s) was varied in the range 1-20 (i.e., for a single hidden layer) and 1:1-10:10 (i.e., for two hidden layers) and the accuracy of the
372 developed model was assessed in terms of the MSE values between the model predictions and the experimental data. An example
373 of the results obtained by this procedure is shown in Figure 1 for the ANN_1 model and the PD method. In this Figure, the ten best
374 (i.e., corresponding to the lowest MSE values) network configurations are shown in a MSE-increasing order. Note that the errors
375 corresponding to all data, validation and testing data sets are shown in order to verify the consistency of the model performance vis-
376 à-vis the different data sets. Each network topology was run 50 times (i.e., 50 different ANNs with the same topology were
377 developed and evaluated) and the average value of MSE was used for comparison, in order to avoid random correlation effects.

Table 5. Experimental conditions of bisphenol-A degradation and apparent kinetic rate constant k_{app} used on the ANN_2 model

pH	Actual amount Ag (%w/w)	BPA (mg/L)	Wavelength (nm)	R[1]	Reaction order *n*	k_{app} experimental	k_{app} predicted (ANN_2 models)	
[2]Pure ZnO photocatalyst							***ANN_2-PD***	***ANN_2-IMP***
10.5	0	10	302	0.973	0.887	4.53E-03	4.53E-03	5.74E-03
10.5	0	10	450	0.988	0.999	6.23E-04	2.27E-04	6.23E-04
7.5	0	10	254	0.992	1.161	2.55E-03	2.79E-03	2.55E-03
2.81	0	10	254	0.999	1.019	3.83E-03	3.78E-03	4.59E-03
4.27	0	10	254	0.999	0.999	3.89E-03	3.78E-03	3.89E-03
9.38	0	10	254	0.986	1.001	4.97E-03	4.92E-03	4.97E-03
10.5	0	10	254	0.999	1.022	7.55E-03	7.44E-03	7.87E-03
7.25	0	20	254	0.999	1.031	1.75E-03	1.73E-03	1.75E-03
8.53	0	20	302	0.990	1.013	1.10E-03	1.21E-03	1.67E-03
8.53	0	20	365	0.999	0.992	2.31E-03	2.41E-03	2.31E-03
Photodeposition method							***ANN_2-PD***	
10.5	1.093	10	254	0.999	1.018	1.02E-02	1.01E-02	
10.5	1.093	10	302	0.999	1.006	1.86E-02	1.52E-02	
10.5	1.093	10	365	0.990	1.002	1.54E-02	1.41E-02	
10.5	1.093	20	254	0.999	1.022	4.97E-03	5.33E-03	
7.51	1.093	40	254	0.982	0.970	1.73E-03	1.24E-03	
10.5	1.147	10	254	0.999	1.024	1.21E-02	1.11E-02	
10.5	1.147	10	302	0.999	1.011	1.85E-02	1.61E-02	
10.5	1.147	10	365	0.999	1.008	1.02E-02	1.01E-02	
10.5	1.147	10	450	0.999	1.046	1.86E-02	1.52E-02	
7.2	1.147	40	254	0.999	0.956	1.54E-02	1.41E-02	
Impregnation method							***ANN_2-IMP***	
10.5	1.203	10	254	0.999	1.007	8.28E-03	9.25E-03	
10.5	1.203	10	302	0.999	0.995	9.37E-03	9.37E-03	
10.5	1.203	10	365	0.999	0.993	1.10E-02	9.02E-03	
10.5	0.366	10	254	0.999	1.006	8.42E-03	8.36E-03	
10.5	0.366	10	302	0.999	0.992	1.22E-02	1.22E-02	
10.5	0.366	10	365	0.999	1.006	1.37E-02	1.17E-02	
10.5	0.366	10	450	0.999	1.009	1.28E-03	1.28E-03	

[1] *Correlation coefficient of the linear regression of the experimental data, as explained in section 2.1.*

[2] *Common experiments, used for the development of both PD and IMP ANN_2 models.*

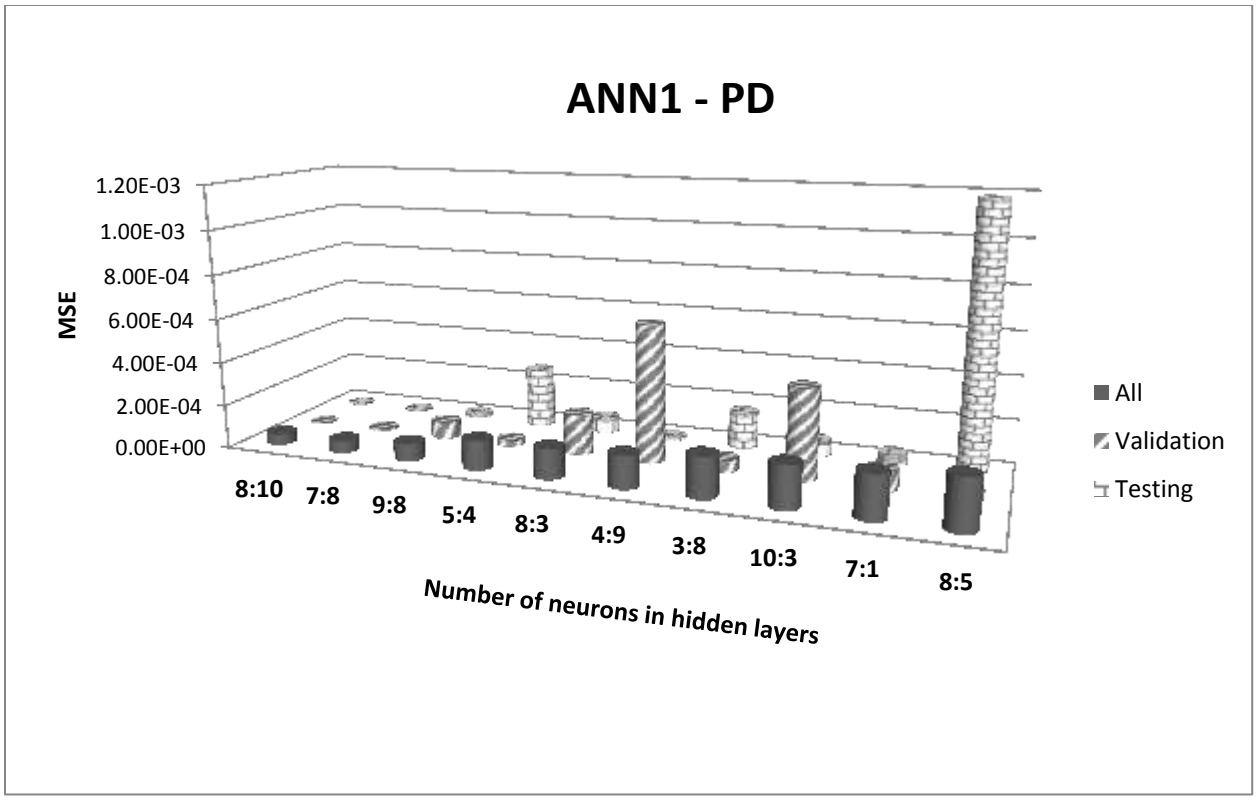

382

383 **Figure 1.** MSE for all data, validation and test datasets as function of neurons in the hidden layer on the network
384 topology for the developed ANN1 model (photodeposition method).

385

386 The numerical data corresponding to Figure 1, as well as the data corresponding to the other
387 three models (i.e., ANN_1-IMP, ANN_2-PD and ANN_2-IMP) are given in Table S.1 of the
388 supplementary material section. The network topologies that were retained according to this
389 procedure are shown in Table 6:

390 **Table 6.** Network topology of the developed models

	Photodeposition – PD	Impregnation – IMP
ANN_1	3:8:10:1	4:9:8:1
ANN_2	3:10:10:1	4:8:10:1

391

392

393

3.2 Evaluation of the ANN models

Neural network models are typically assessed, in terms of their accuracy in simulating the experimental data, by plotting the model response with respect to the experimental measurements. A comparison of the points of such plots with the diagonal (i.e., the linear curve corresponding to y=x) reveals the accuracy of the developed model. Figures 2 and 3 depict such plots for the ANN_1 and ANN_2 models, respectively. In these plots, the all data and test data sets are shown in order to reveal the accuracy of the model with respect to all available data, including the training data for which a higher accuracy is expected, as well as with respect only to the test data, which represent a subset of the available data that has not been used during the model training process. The value of the correlation coefficient, R, of the linear regression of the data is also shown on the plots. It can be seen that the ANN_1 model exhibits higher accuracy than the ANN_2 model, which seems to under-predict the experimental values at the high-values domain of k_{app} but, in general, remains quite accurate as well. This can be partially attributed to the smaller size of available experimental data for the second model. The values of the experimental data used for the development of the models and the respective model predictions are also given in Tables 4 and 5. Note that, for the training of the models of the photodegradation experiments, ANN_2, the target values of the experimental apparent rate constant were transformed to their log values, in order to avoid a variation over several orders of magnitude. Nevertheless, in all graphical and numerical results presented in this paper, the original non-transformed values are shown for reasons of simplicity.

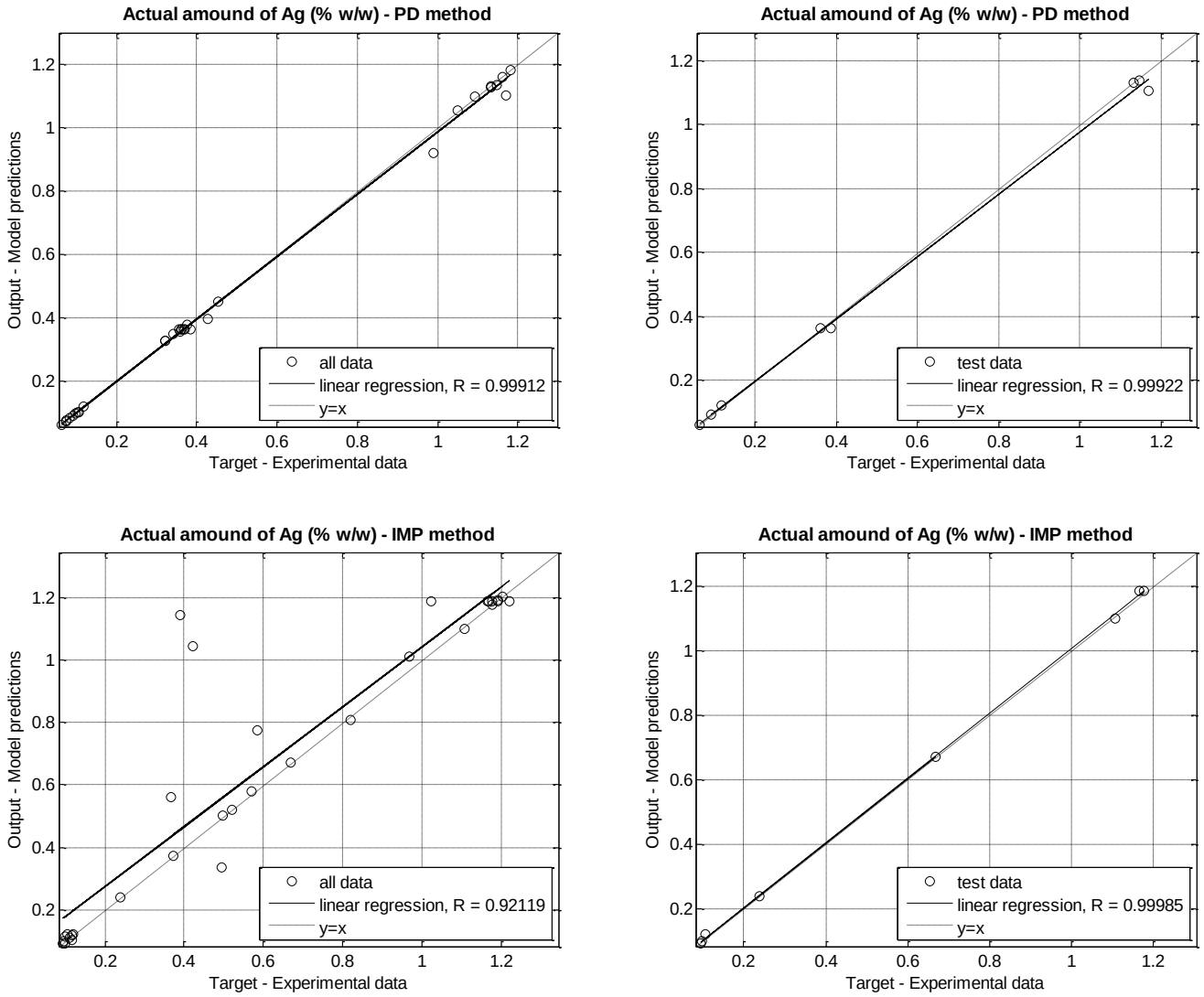

414 **Figure 2.** Regression plots of the experimental data (all data and test data sets) versus model predicted values for
415 the developed neural network models ANN_1-PD (top) and ANN_1-IMP (bottom).
416

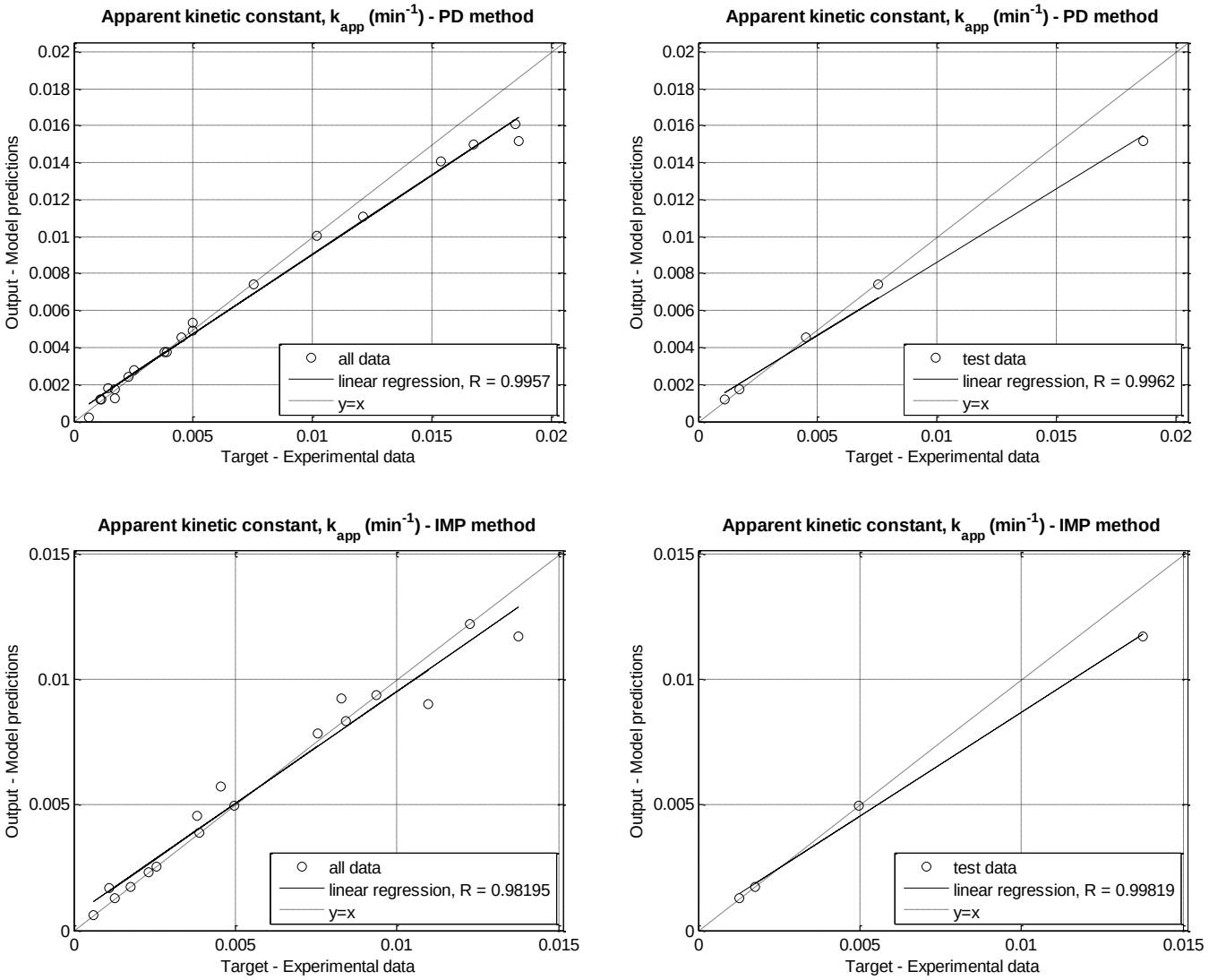

417 **Figure 3.** Regression plots of the experimental data (all data and test data sets) versus model predicted values for
418 the developed neural network models ANN_2-PD (top) and ANN_2-IMP (bottom).
419

3.3 Analysis of the model results

Once the ANN models have been successfully developed and validated, they can be directly implemented, using input values that do not necessarily correspond to the experimentally tested conditions, in order to assess the effect of the different conditions of each sub-process (i.e., the catalyst synthesis and the degradation tests) to the respective response of interest (i.e., the actual amount of attached Ag on the photocatalyst and the apparent degradation rate constant, respectively). In this respect, Figures 4a-4f show the effect of pH and actual silver content on the degradation rate of BPA, under different conditions of BPA amount and light wavelength, as produced by the ANN_2-PD model. An initial observation is that the response surfaces are highly irregular, not displaying a clear increasing or decreasing effect. It should be noted at this point that the presented curves can only serve to acquire a general idea about the different trends that the model might display with respect to the variation of certain inputs. They cannot be used to identify specific points or values with accuracy since the viewpoint angle and the graphical interpolation used for their creation may lead to errors.

Concerning the effect of pH, it can be seen that, as pH increases the values of k_{app} initially increase, reaching a maximum within the range of pH values 6-9, and then decrease. This effect is particularly obvious in Figures 4d-4f. The pH is an important factor in photocatalysis since it affects the surface charges of both the photocatalyst and the contaminant as follows. In the vicinity above neutral pH_{PZC}=8.3 (i.e., value of neutral surface charges for ZnO), hydroxyl-compounds of zinc such as $ZnOH^+$, $Zn(OH)_2$, and $Zn(OH)_3^-$ are formed in the solution and they interact with the undissociated BPA ($HO\text{-}C_{15}H_{14}\text{-}OH$) toward its oxidation. Below this value, an

increase in the hydroxyl ion ($^{-}$OH) concentration and, subsequently, to the hydroxyl radical (●OH) concentration leads to the oxidation of BPA. Comparable results have been reported on the degradation efficiency of BPA by pure ZnO by Rahman et al. (2005), who reported 80% degradation efficiency of 100 mg/L of BPA in the pH range of 2 to 8.5, and a significant decrease to 60% at pH 11. Also, Clament Sagaya Selvam et al. (2013) reported the complete degradation of 200 mg/L of BPA at pH 8 and a subsequent decrease of the degradation efficiency at pH values above 9.

Figure 4a: BPA = 22 mg/l and UV = 254 nm

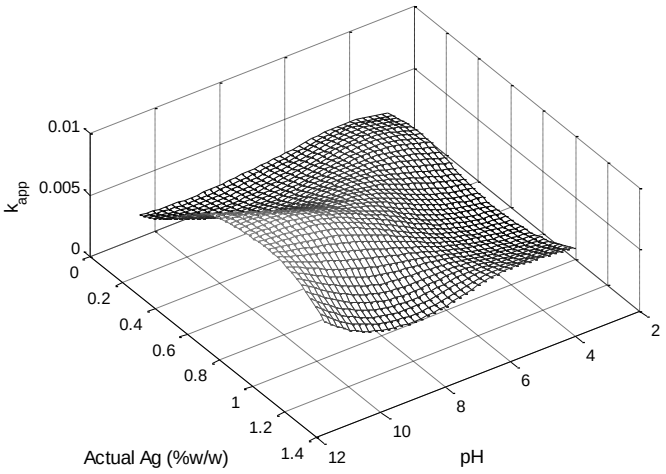

Figure 4b: BPA = 28 mg/l and UV = 254 nm

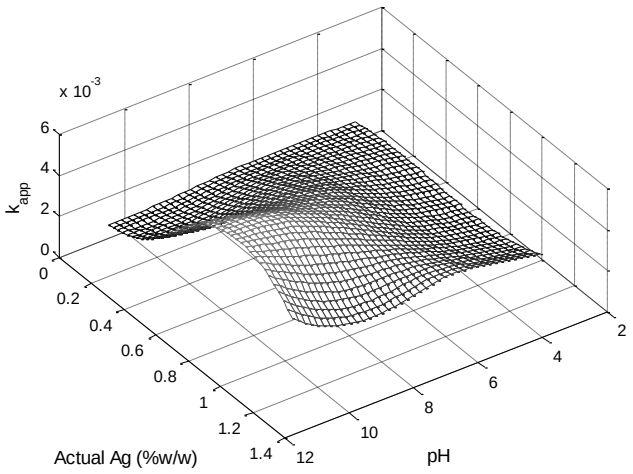

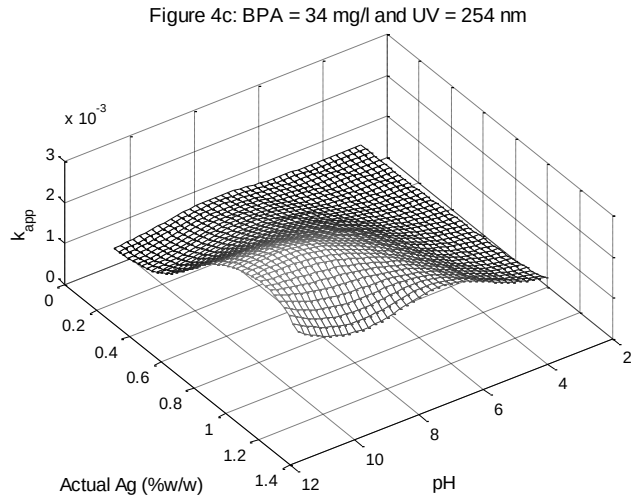

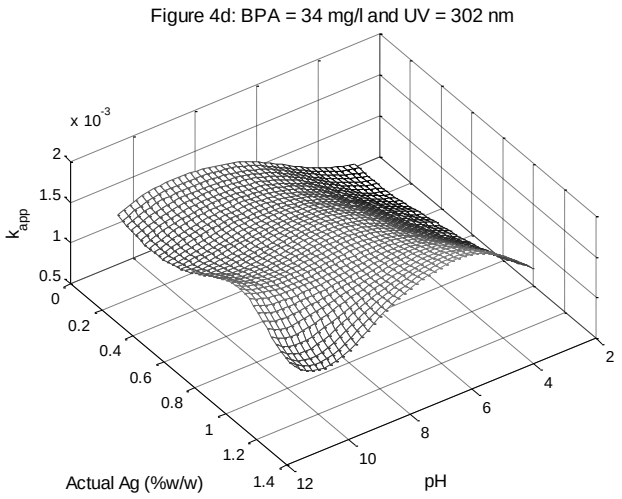

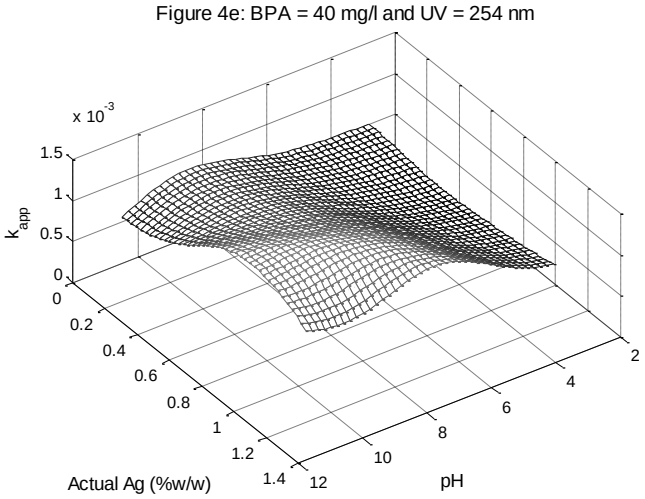

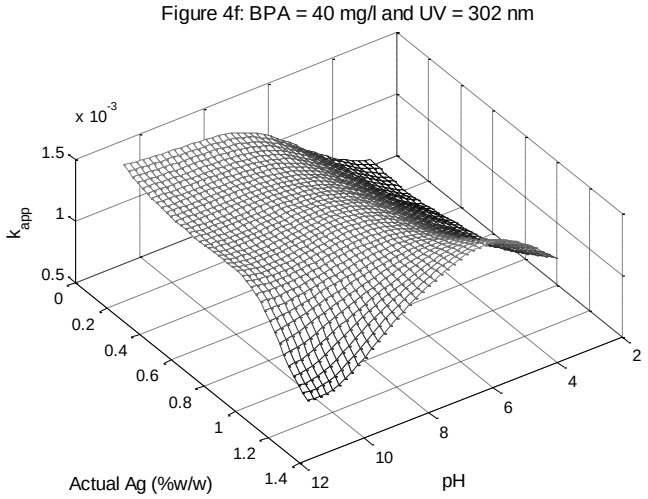

Figure 4: Effect of pH and actual silver content (% w/w) on the apparent degradation rate constant under different conditions of BPA content and UV wavelength, as simulated by the ANN_2-PD model.

On the other hand, the effects of BPA concentration and UV wavelength are not so evident. Nevertheless, the initial contaminant concentration seems to display an inversely proportional effect on the values of k_{app}, since they seem to be decreasing at higher BPA concentrations. This effect can be partially explained by an absorbance of the UV light (at 255 and 277 nm) by BPA molecules. This way, the activation of the photocatalyst surface is reduced thus producing a *screening effect* of the BPA molecules towards the UV light penetration.

A similar effect for all factors can be observed for the impregnation model, ANN_2-IMP, as well. Four representative surfaces are shown in Figures 5a-5d, under different conditions of BPA content and light wavelength. As can be seen, the value of k_{app} displays once more a maximum around the middle of the pH and BPA concentration domains and decreases with increasing BPA concentration.

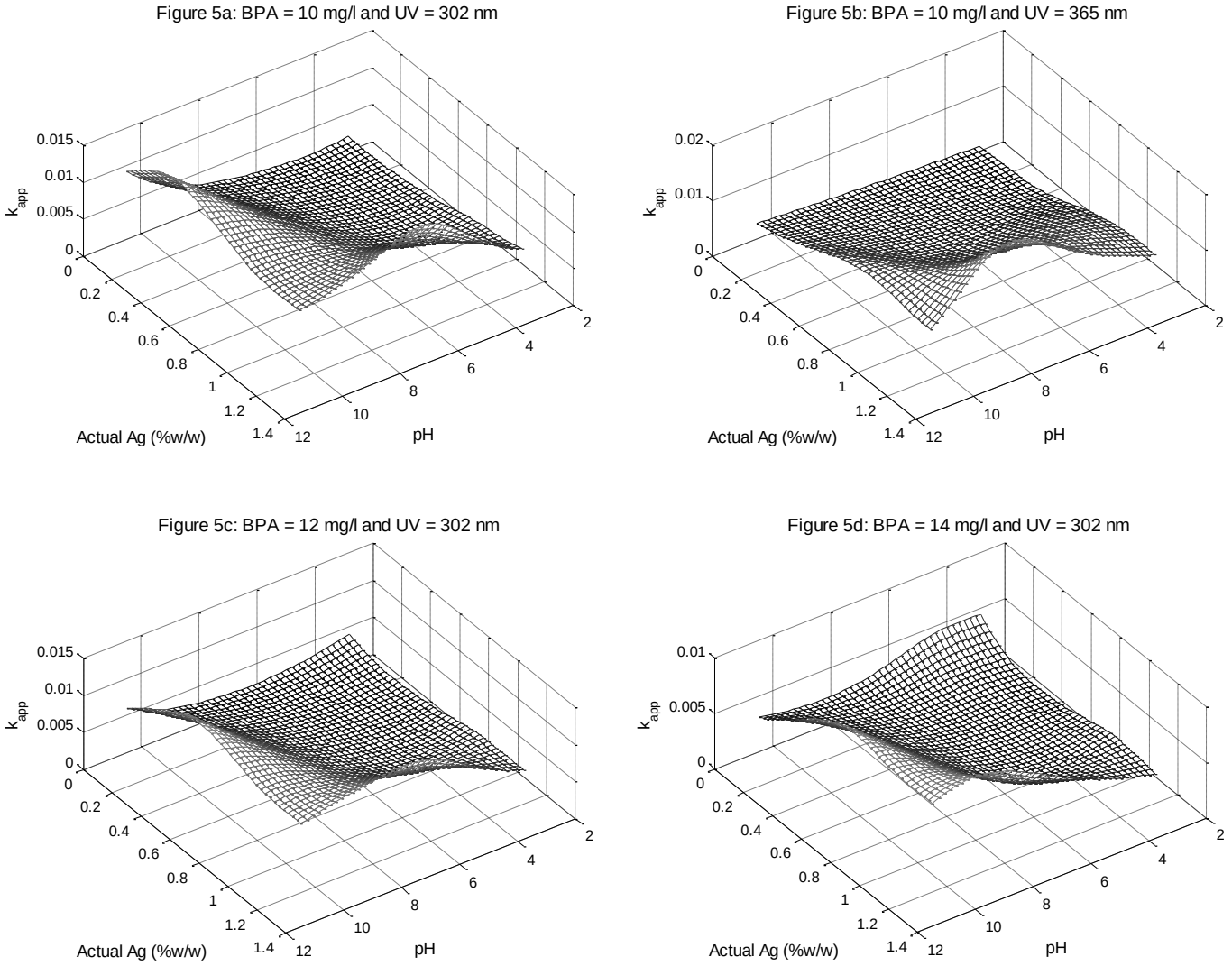

Figure 5: Effect of pH and actual silver content (% w/w) on the apparent degradation rate constant under different conditions of BPA content and UV wavelength, as simulated by the ANN_2-IMP model.

464 Concerning the first model, ANN_1, a similar analysis can be made on the effects of the catalyst
465 synthesis conditions on the overall functionalization degree, FD, defined as the ratio of the
466 actual amount of silver on the catalyst particles over the nominal amount of silver used during
467 the catalyst synthesis. In Figures 6a and 6b, two surface plots, similar to the ones previously
468 depicted for ANN_2, are shown corresponding to the photodeposition method and to two
469 different values of nominal amount of silver. The corresponding plots for the impregnation
470 method are depicted in Figures 6c and 6d. As can be seen, there is no significant variation of FD
471 with respect to pH and time when the photodeposition method is implemented. On the other
472 hand, the reaction time seems to have an overall positive effect on the FD values and to display
473 a maximum around 150 min, when the impregnation method is used.
474 The effect of pH seems to vary with the time of reaction and the nominal AG amount, especially
475 for the photodeposition method. At the same time, an excess nominal amount of silver does not
476 seem to display a positive effect on the functionalization degree when the impregnation
477 method is implemented, which is particularly obvious in Figure 6d. It should be noted at this
478 point that the experimental values of FD that are higher than 1 are due to experimental
479 sampling and titration errors, as explained in (Jasso-Salcedo et al., 2014). As a consequence it is
480 normal that the developed neural network model, which was trained on the basis of these
481 experimental values, provides responses that result in values of FD higher than 1.

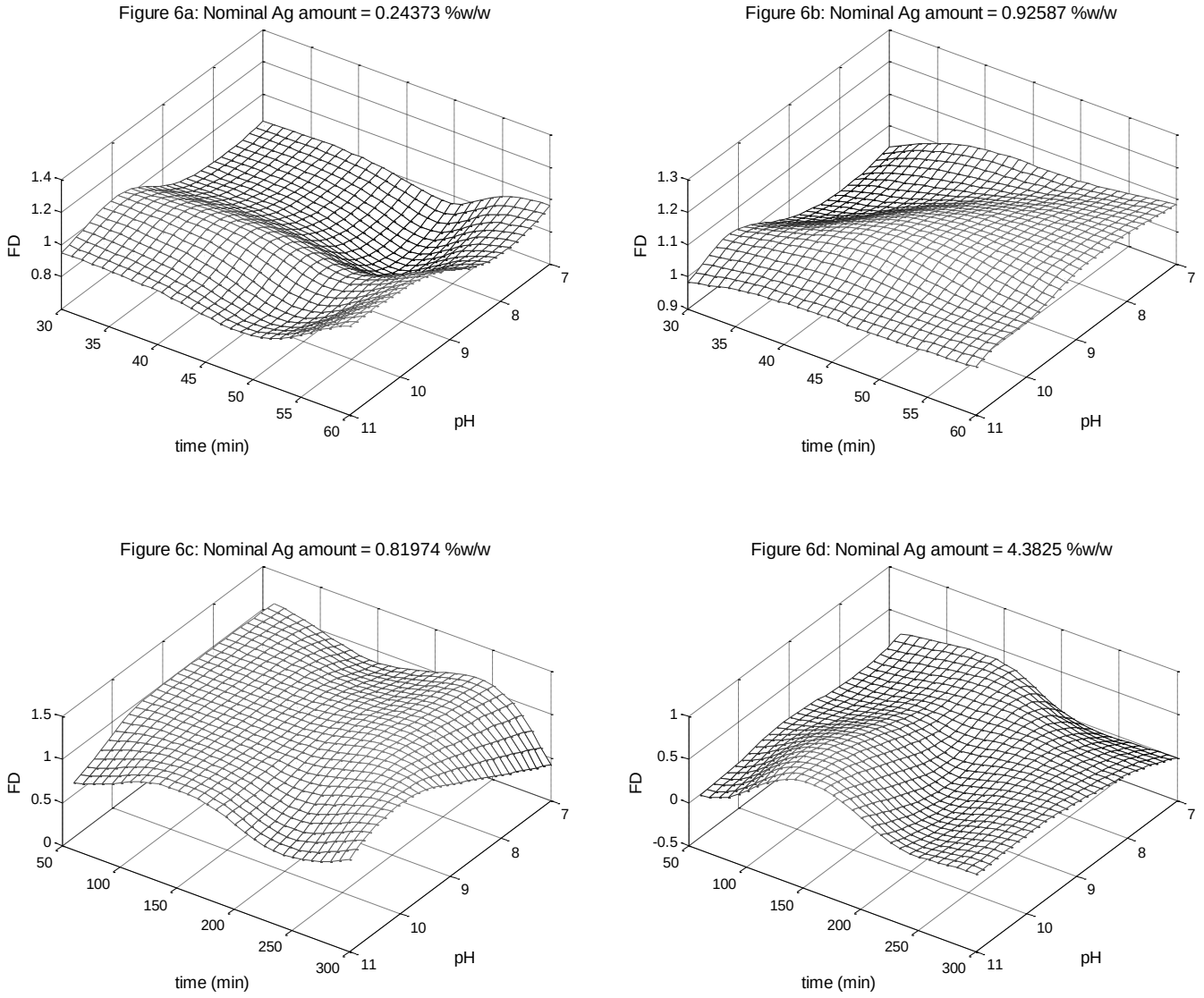

Figure 6: Effect of pH and nominal silver content (% w/w) on the functionalization degree (i.e., the ratio of actual to nominal amount of Ag) under different values of nominal Ag amount as simulated by the ANN_1-PD (a, b) and ANN_1-IMP (d, c) models.

3.4 Optimization step 1 - apparent kinetic rate constant, k_{app}

Given the nature of the photodegradation process and the definition of the output of the process on the basis of the apparent kinetic rate constant of a first-order degradation reaction, it becomes evident that the desired value of this constant is the maximal possible value it could

attain, as this will lead to a faster degradation of a maximum amount of BPA. Hence, the first step of the optimization study, on the basis of ANN_2, was the solution of a maximization problem in terms of the conditions of the photodegradation process, namely the actual amount of attached AgNPs, the pH, the BPA concentration and the light wavelength. The deployment of an EA for the solution of this problem for both methods of photocatalyst synthesis resulted in the sets of optimal conditions shown in Table 7. Note that, for the EA algorithm, the following parameters were used: the size of the population was set to 1000 individuals, the survival rate was set to 70% and the mutation rate to 10%. The program was entirely written and run on MATLAB (version 8.3.0.532; academic license) while the convergence of the algorithm was tested in terms of a tolerance in the relative difference between the best and worst criterion values of each generation, set in the order of 1%.The CPU time required for every optimization run was in the order of 30 s on a 2x2.4 GHz Intel® Xeon® Workstation.

Table 7: Results of the first optimization step on the maximization of k_{app}

Optimal photodegradation conditions for the photodeposition method ($k_{app,max}$ = 0.0383 min^{-1})			
Actual amount Ag, %w/w	pH (initial value)	BPA concentration, mg/L	Wavelength, nm
1.10	*6.7*	*10.8*	*330*
Optimal photodegradation conditions for the impregnation method ($k_{app,max}$ = 0.0167 min^{-1})			
Actual amount Ag, %w/w	pH (initial value)	BPA concentration, mg/L	Wavelength, nm
0.78	*10.1*	*10.2*	*358*

In order to follow the evolution of the optimization and to verify its convergence around one (or more) optimal(s), one can plot the positions of a number of 'best' (i.e., top ranked) individuals, corresponding to an equal number of optimal conditions, along different generations of the optimization procedure. In Figures 7a-7d, a set of 50 optimal conditions is depicted, as calculated by the EA optimization of the ANN_2-PD model.

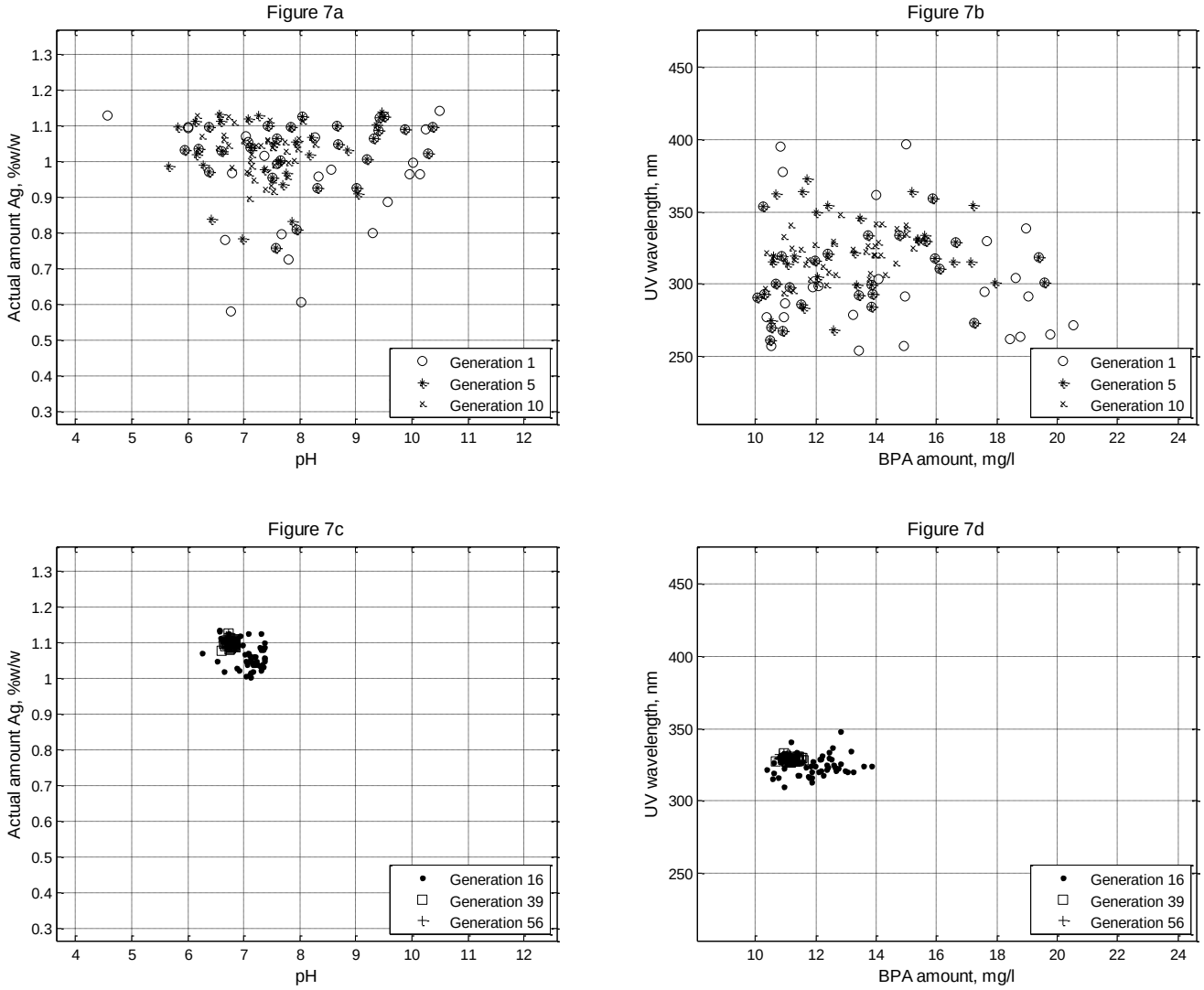

Figure 7: Presentation of the 50 optimal conditions in terms of the actual amount of Ag and pH (a, c) and the UV wavelength and the BPA amount (b, d), as predicted by the EA optimization on the basis of the ANN_2-PD model after 1, 5 and 10 generations (a, b) as well as after 16, 39 and 56 generations (c, d).

Since there are four different factors for this model, two plots are produced for each generation, one corresponding to the optimal values of the actual amount of silver and pH and another corresponding to the optimal values of the UV wavelength and the initial BPA amount. The same Figures have been plotted for three different generations at the early stages of the optimization (i.e., generations 1, 2 and 10, cf. Figures 7a and 7b) as well as for three generations

519 at the middle and final stages of the optimization (i.e., generations 16, 39 and 56, cf. Figures 7c
520 and 7d). This illustration reveals the convergence of the optimization around a unique set of
521 optimal conditions (cf. Table 7). In this specific case, the convergence was achieved after 56
522 iterations, according to the convergence criterion defined earlier in this Section. Note that the
523 predicted optimal value of k_{app} is significantly increased with respect to the experimentally
524 measured values.

525 Figures 8a-8d present the corresponding plots of the same optimization problem but for the
526 impregnation method (i.e., on the basis of ANN_2-IMP). In this case, several local maxima seem to
527 exist so the optimization does not converge around one single set of optimal conditions. The
528 conditions reported in Table 7 are the ones that lead to the maximum attaint value of the
529 apparent rate constant and correspond to the set of points located on the right in Figure 8c and
530 on the top left in Figure 8d. In any case, this method seems to lead to significantly lower optimal
531 values of the rate constant, in comparison to the photodeposition method.

532

Figure 8a

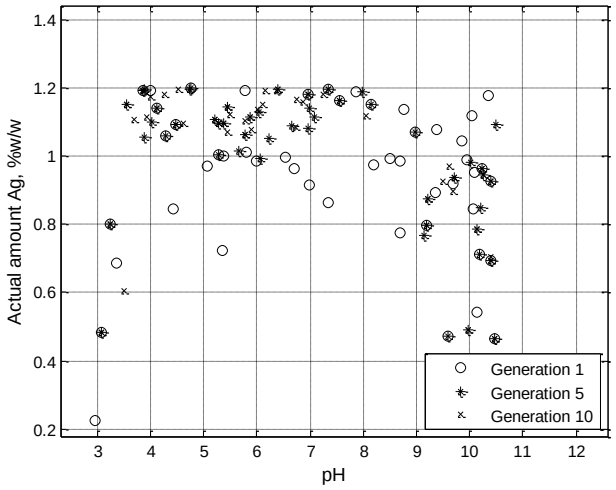

Figure 8b

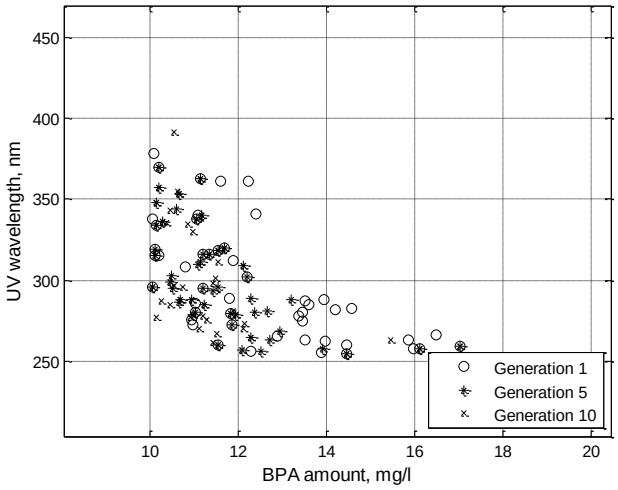

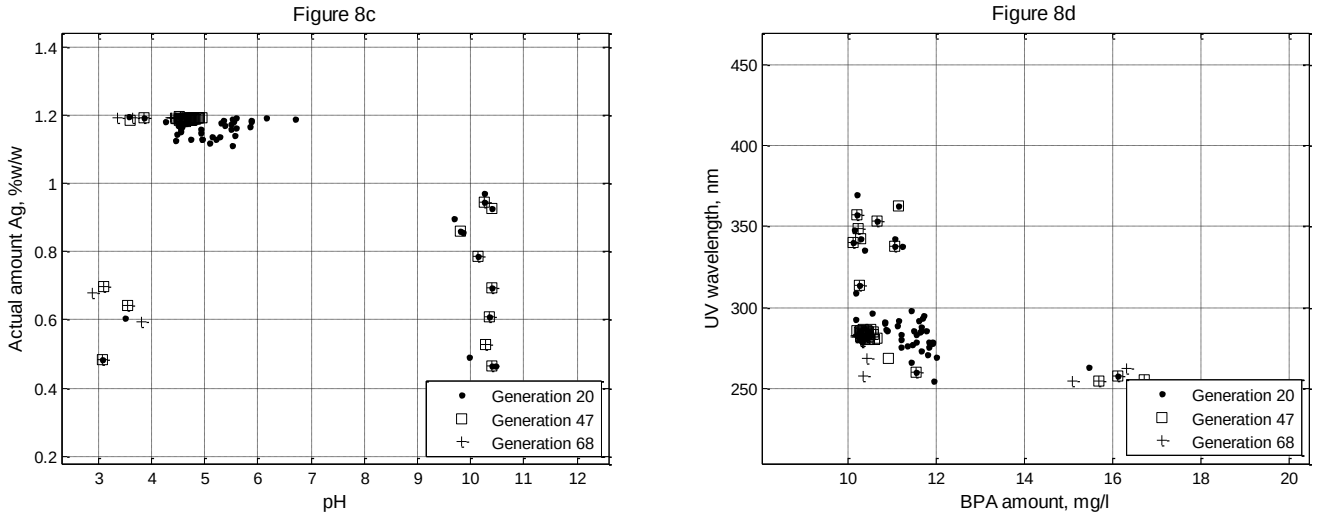

533 **Figure 8:** Presentation of the 50 optimal conditions in terms of the actual amount of Ag and pH (a, c) and the UV
534 wavelength and the BPA amount (b, d), as predicted by the EA optimization on the basis of the ANN_2-IMP model
535 after 1, 5 and 10 generations (a, b) as well as after 20, 47 and 68 generations (c, d).

536

537 ## 3.5 Optimization step 2 - actual amount of silver in the ZnO photocatalyst

538 On the basis of the optimal amount of AgNPs defined by the previous optimization step, a
539 second optimization run was carried out in order to define the conditions that would result in
540 the synthesis of a photocatalyst with this optimal amount of silver nanoparticles. So, in this
541 case, the goal was to minimize the objective function defined by the absolute difference
542 between the model response (i.e., the actual Ag amount) and the desired Ag amount, as this
543 was defined in the previous optimization step. This second step of the optimization study was
544 based on ANN_1 and the results of the EA that was deployed for the solution of this problem are
545 shown in Table 8. In both cases, the error between the desired and attained value was inferior
546 to 0.01%, significantly lower than the associated experimental error of the measurements.

547

548

549

550 **Table 8**: Results of the 2nd optimization step on the synthesis of a photocatalyst with a desired content of AgNPs

Optimal photocatalyst synthesis conditions for the photodeposition method (Actual Ag %w/w = 1.10)		
Nominal amount Ag, %w/w	pH	Time, min
1.00	*9.5*	*48*
Optimal photocatalyst synthesis conditions for the impregnation method (Actual Ag %w/w = 0.78)		
Nominal amount Ag, %w/w	pH	Time, min
0.69	*8.5*	*214*

551

552 The respective 2D plots of the evolution of the 50 optimal conditions in terms of the model
553 factors are presented in Figures 9a-9d and 10a-10d, for the photodeposition and the
554 impregnation methods respectively. Note that, as the number of factors is limited to three in
555 this case, both couples that are used in the plots contain pH as one of the factors.

Figure 9a

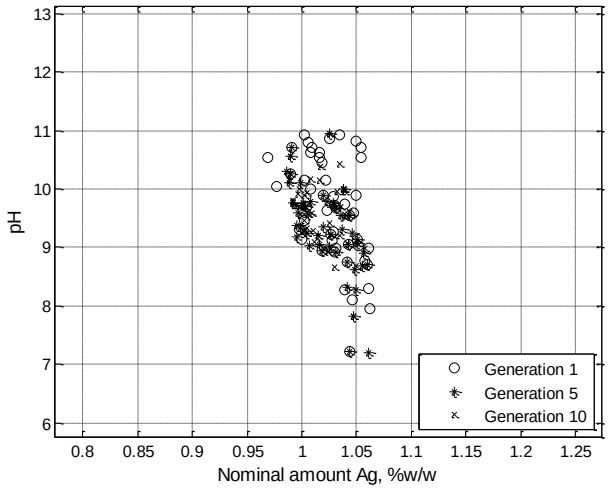

Figure 9b

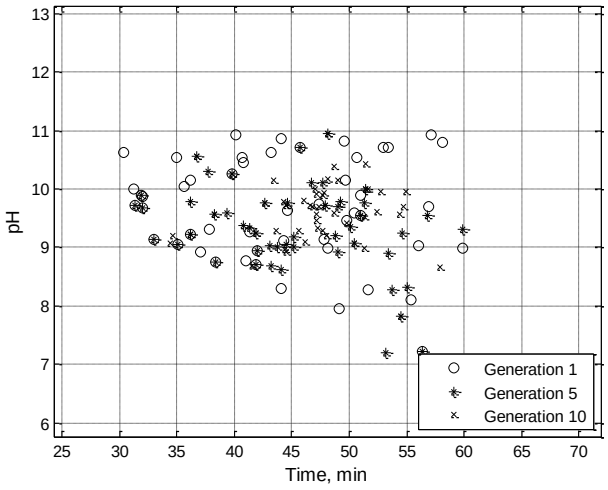

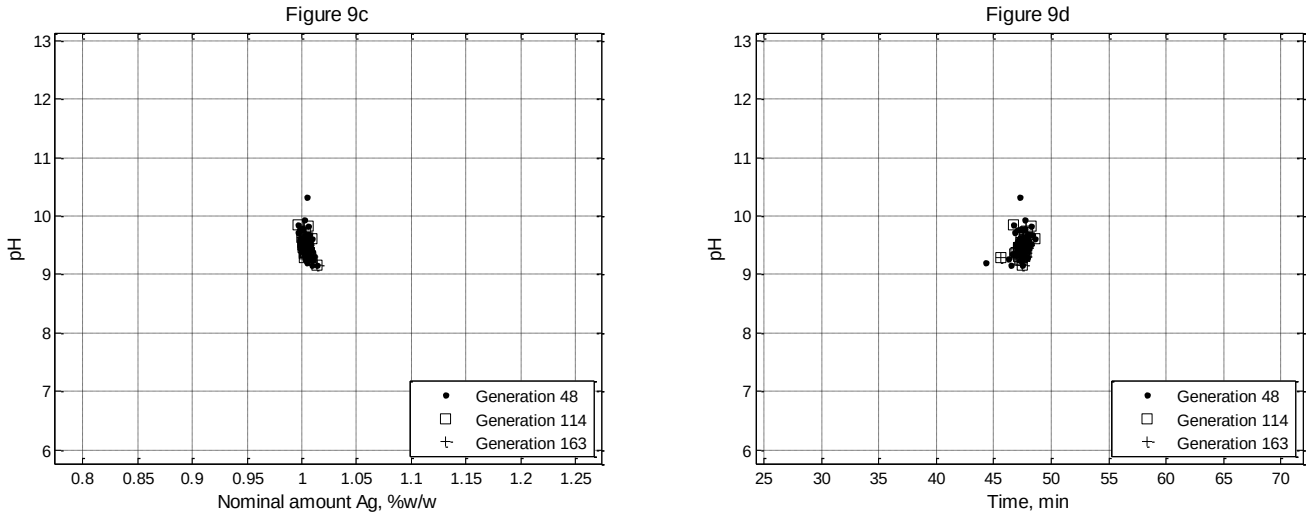

Figure 9: Presentation of the 50 optimal conditions in terms of the nominal amount of Ag and pH (a, c) and the reaction time and pH (b, d), as predicted by the EA optimization on the basis of the ANN_1-PD model after 1, 5 and 10 generations (a, b) as well as after 48, 114 and 163 generations (c, d).

The results of these optimization runs are quite similar to the first optimization runs as, once again, the impregnation method seems to provide several alternatives as local minima, especially in terms of the value of the pH, as becomes evident in Figures 10a and 10c. The photodeposition method, on the other hand, has a clear minimum of the objective function that is identified by the EA algorithm already somewhere between the 10^{th} and 48^{th} iteration, despite the fact that the algorithm requires more than 160 iterations to meet the convergence criterion. Finally, a paradox is observed in both optimization results since the optimal nominal amount of Ag is lower than the desired actual amount of Ag. Once again, this is due to the fact that the models have been trained with experimental data containing such discrepancies, which are caused by the experimental error associated with the experimental protocol and the analytical method (Jasso-Salcedo et al., 2014). This should not be interpreted as an error associated with the modeling framework or the optimization approach.

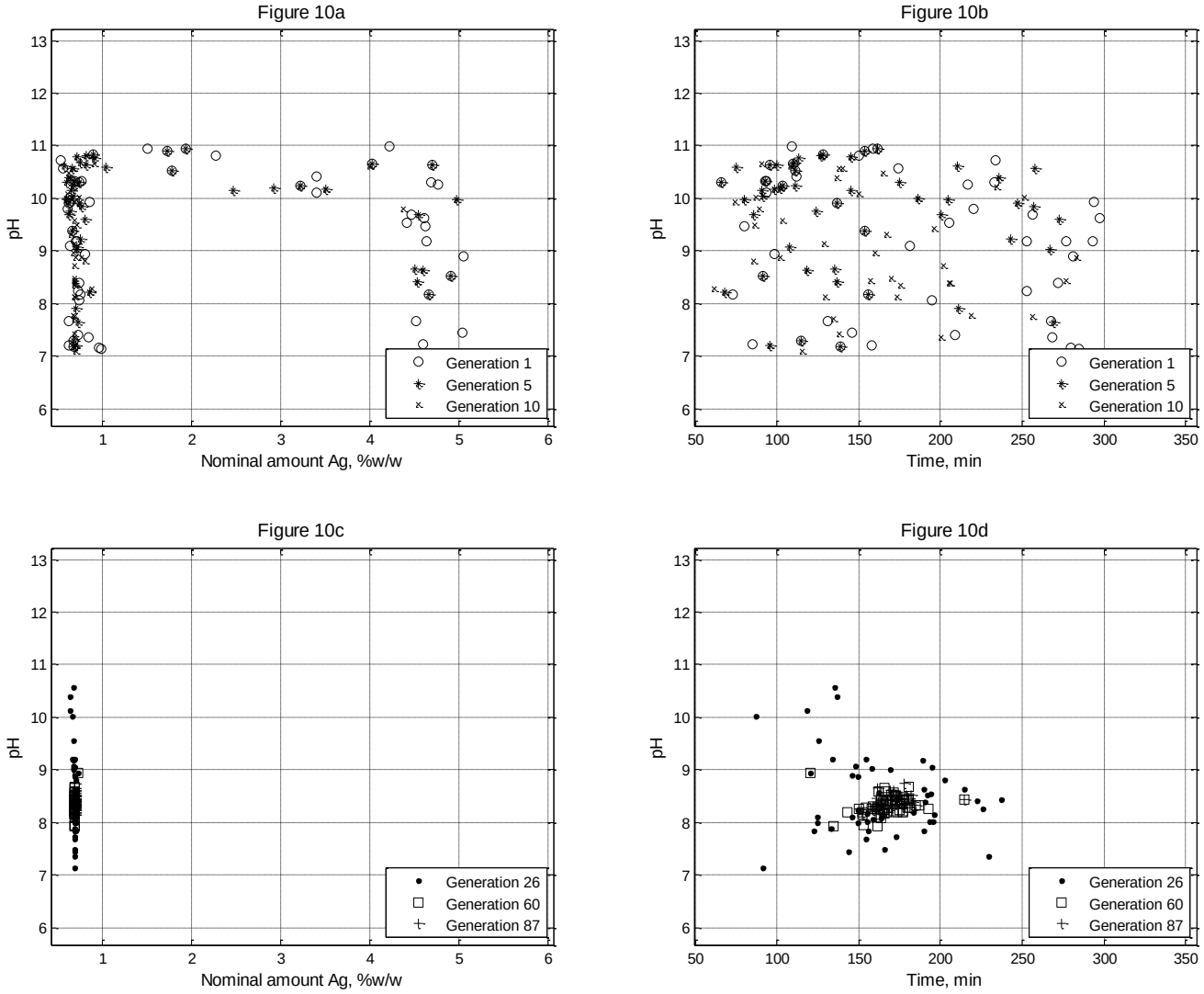

572 **Figure 10:** Presentation of the 50 optimal conditions in terms of the nominal amount of Ag and pH (a, c) and the
573 reaction time and pH (b, d), as predicted by the EA optimization on the basis of the ANN_1-IMP model after 1, 5 and
574 10 generations (a, b) as well as after 26, 60 and 87 generations (c, d).

575

576 # 4 Conclusions

577 In the present work, a modeling framework on the basis of Artificial Neural Networks was
578 presented for the simulation of the effects of two important stages of a photocatalytic process,
579 namely the catalyst synthesis and the photodegradation experiments, on the final

photodegradation performance of the synthesized photocatalyst. In this respect, a two-stage ANN model was developed, connected by means of introducing the response of the first model as a factor to the second model. The developed models were subsequently introduced in an optimization study, carried out with the aid of an evolutionary algorithm and comprised also of two steps. Through this integrated approach, it has been possible to study simultaneously the effects of a series of important conditions associated with two totally distinct stages of the process and to connect the initial photocatalyst synthesis conditions with its final photodegradation performance.

By means of the developed models, the effects of pH, nominal amount of silver nanoparticles introduced in the suspension and reaction time were assessed in terms of their effects on the actual amount of silver nanoparticles that are finally retained on the ZnO surface. At the same time, this amount of attached silver along with the pH, the light wavelength and the initial contaminant amount present in the photodegradation experiments were studied in terms of their effect on the photodegradation performance of the synthesized photocatalyst. This performance was associated with an apparent rate constant, thus eliminating the time from the factors of the photodegradation tests.

The decoupling of these two processes that was proposed in this study allowed a better understanding of the nature of the indisputable indirect bond that exists between them. In this respect, it has been shown that an intermediate quality criterion of the photocatalyst, namely the actual amount of silver attached to the ZnO surface that, in turn, can only be controlled by the photocatalyst synthesis conditions, displays a direct effect on its photodegradation performance. Finally, by investigating two different methods of the photocatalyst synthesis,

602 namely a photodeposition and an impregnation method, the study has also demonstrated that
603 it can display an important effect on the final photodegradation efficiency of the photocatalyst.
604
605 **Acknowledgements.**
606 This work was supported by CONACYT and the French Ministry of Education and Research
607 (scholarship PCP/RUI-004-12 granted to AB Jasso-Salcedo).
608 ## References
609 Amani-Ghadim, A. R., & Seyed Dorraji, M. S. (2015). Modeling of photocatalyatic process on
610 synthesized ZnO nanoparticles: Kinetic model development and artificial neural networks.
611 Applied Catalysis B: Environmental, 163, 539-546.
612 Antonopoulou, M., & Konstantinou, I. (2013). Optimization and Modeling of the Photocatalytic
613 Degradation of the Insect Repellent DEET in Aqueous TiO2Suspensions. CLEAN - Soil, Air,
614 Water, 41, 593-600.
615 Antonopoulou, M., Papadopoulos, V., & Konstantinou, I. (2012). Photocatalytic oxidation of
616 treated municipal wastewaters for the removal of phenolic compounds: optimization and
617 modeling using response surface methodology (RSM) and artificial neural networks (ANNs).
618 Journal of Chemical Technology and Biotechnology, 87, 1385-1395.
619 Asl, S. K., Sadrnezhaad, S. K., Rad, M. K., & Üner, D. (2012). Comparative photodecolorization of
620 red dye by anatase, rutile (TiO_2), and wurtzite (ZnO) using response surface methodology.
621 Turkish Journal of Chemistry, 36, 121-135.
622 Babaei, A., Mesdaghiniai, A., Haghighi, N. J., Nabizadeh, R., & Mahvi, A. (2011). Modeling of
623 nonylphenol degradation by photo-nanocatalytic process via multivariate approach. Journal
624 of Hazardous materials, 185, 1273-1279.
625 Behnajady, M. A., & Eskandarloo, H. (2015). Preparation of TiO2 nanoparticles by the sol–gel
626 method under different pH conditions and modeling of photocatalytic activity by artificial
627 neural network. Research on Chemical Intermediates, 41, 2001-2017.
628 Bohdziewicz, J., Kudlek, E., & Dudziak, M. (2016). Influence of the catalyst type (TiO2 and ZnO)
629 on the photocatalytic oxidation of pharmaceuticals in the aquatic environment. Desalination
630 and water treatment, 57, 1552-1563.
631 Camargo, M., Morel, L., Fonteix, C., Hoppe, S., Hu, G. H., & Renaud, J. (2011). Development of
632 new concepts for the control of polymerization processes: Multiobjective optimization and
633 decision engineering. II. Application of a Choquet integral to an emulsion copolymerization
634 process. Journal of Applied Polymer Science, 120, 3421-3434.
635 Cheng, B., & Titterington, D. M. (1994). Neural Networks: A Review from a Statistical
636 Perspective. Statistical Science, 9, 49-54.

637 Clament Sagaya Selvam, N., Judith Vijaya, J., & John Kennedy, L. (2013). Comparative studies on
638 influence of morphology and La doping on structural, optical, and photocatalytic properties
639 of zinc oxide nanostructures. Journal of Colloid and Interface Science, 407, 215-224.
640 Das, L., Maity, U., & Kumar Basu, J. (2014). The photocatalytic degradation of carbamazepine
641 and prediction by artificial neural networks. Process Safety and Environmental Protection, 92,
642 888-895.
643 Delnavaz, M. (2015). Application of Artificial Neural Networks for Prediction of Photocatalytic
644 Reactor. Water Environment Research, 87, 113-122.
645 Dutta, S., Parsons, S. A., Bhattacharjee, C., Bandhyopadhyay, S., & Datta, S. (2010). Development
646 of an artificial neural network model for adsorption and photocatalysis of reactive dye on
647 TiO2 surface. Expert Systems with Applications, 37, 8634-8638.
648 Esplugas, S., Bila, D. M., Krause, L. G. T., & Dezotti, M. (2007). Ozonation and advanced oxidation
649 technologies to remove endocrine disrupting chemicals (EDCs) and pharmaceuticals and
650 personal care products (PPCPs) in water effluents. Journal of Hazardous materials, 149, 631-
651 642.
652 Fernández, R. L., McDonald, J. A., Khan, S. J., & Le-Clech, P. (2014). Removal of pharmaceuticals
653 and endocrine disrupting chemicals by a submerged membrane photocatalysis reactor
654 (MPR). Separation and Purification Technology, 127, 131-139.
655 Ferreira, S. L. C., Bruns, R. E., Ferreira, H. S., Matos, G. D., David, J. M., Brandão, G. C., da Silva, E.
656 G. P., Portugal, L. A., dos Reis, P. S., Souza, A. S., & dos Santos, W. N. L. (2007). Box-Behnken
657 design: An alternative for the optimization of analytical methods. Analytica Chimica Acta,
658 597, 179-186.
659 Flint, S., Markle, T., Thompson, S., & Wallace, E. (2012). Bisphenol A exposure, effects, and
660 policy: A wildlife perspective. Journal of Environmental Management, 104, 19-34.
661 Fonteix, C., Bicking, F., Perrin, E., & Marc, I. (1995). Haploid and diploid algorithms, a new
662 approach for global optimization: compared performances. International Journal of Systems
663 Science, 26, 1919-1933.
664 Frontistis, Z., Daskalaki, V. M., Hapeshi, E., Drosou, C., Fatta-Kassinos, D., Xekoukoulotakis, N. P.,
665 & Mantzavinos, D. (2012). Photocatalytic (UV-A/TiO2) degradation of 17α-ethynylestradiol in
666 environmental matrices: Experimental studies and artificial neural network modeling. Journal
667 of Photochemistry and Photobiology A: Chemistry, 240, 33-41.
668 Georgakis, C. (2013). Design of Dynamic Experiments: A Data-Driven Methodology for the
669 Optimization of Time-Varying Processes. Industrial & Engineering Chemistry Research, 52,
670 12369-12382.
671 Georgekutty, R., Seery, M. K., & Pillai, S. C. (2008). A Highly Efficient Ag-ZnO Photocatalyst:
672 Synthesis, Properties, and Mechanism. The Journal of Physical Chemistry C, 112, 13563-
673 13570.
674 Ghanbary, F., Modirshahla, N., Khosravi, M., & Behnajady, M. A. (2012). Synthesis of TiO2
675 nanoparticles in different thermal conditions and modeling its photocatalytic activity with
676 artificial neural network. Journal of Environmental Sciences, 24, 750-756.
677 Haykin, S. (1994). Neural Networks: A Comprehensive Foundation (Vol. 2): Macmillan.
678 Heiligers, B. (1994). E-optimal designs in weighted polynomial regression. The Annals of
679 Statistics, 917-929.

Jasso-Salcedo, A. B., Meimaroglou, D., Hoppe, S., Pla, F., & Escobar-Barrios, V. A. (2016). Surface modification and immobilization in poly (acrylic acid) of Ag/ZnO for photocatalytic degradation of endocrine-disrupting compounds. Journal of Applied Polymer Science, 133.

Jasso-Salcedo, A. B., Palestino, G., & Escobar-Barrios, V. A. (2014). Effect of Ag, pH, and time on the preparation of Ag-functionalized zinc oxide nanoagglomerates as photocatalysts. Journal of Catalysis, 318, 170-178.

Khataee, A. R., Fathinia, M., Zarei, M., Izadkhah, B., & Joo, S. W. (2014). Modeling and optimization of photocatalytic/photoassisted-electro-Fenton like degradation of phenol using a neural network coupled with genetic algorithm. Journal of Industrial and Engineering Chemistry, 20, 1852-1860.

Khataee, A. R., & Kasiri, M. B. (2010). Artificial neural networks modeling of contaminated water treatment processes by homogeneous and heterogeneous nanocatalysis. Journal of Molecular Catalysis A: Chemical, 331, 86-100.

Kiattisaksiri, P., Khamdahsag, P., Khemthong, P., Pimpha, N., & Grisdanurak, N. (2015). Photocatalytic degradation of 2, 4-dichlorophenol over Fe-ZnO catalyst under visible light. Korean Journal of Chemical Engineering, 32, 1578-1585.

Kiransan, M., Khataee, A., Karaca, S., & Sheydaei, M. (2015). Artificial neural network modeling of photocatalytic removal of a disperse dye using synthesized of ZnO nanoparticles on montmorillonite. Spectrochimica Acta Part A: Molecular and Biomolecular Spectrosctroscopy, 140, 465-473.

Kıransan, M., Khataee, A., Karaca, S., & Sheydaei, M. (2015). Synthesis of Zinc Oxide Nanoparticles on Montmorillonite for Photocatalytic Degradation of Basic Yellow 28: Effect of Parameters and Neural Network Modeling. Current Nanoscience, 11, 343-353.

Klečka, G. M., Staples, C. A., Clark, K. E., van der Hoeven, N., Thomas, D. E., & Hentges, S. G. (2009). Exposure analysis of bisphenol A in surface water systems in North America and Europe. Environmental Science & Technology, 43, 6145-6150.

Lee, K. M., & Hamid, S. B. A. (2015). Simple response surface methodology: Investigation on advance photocatalytic oxidation of 4-chlorophenoxyacetic acid using UV-active ZnO photocatalyst. Materials, 8, 339-354.

Meireles, M. R., Almeida, P. E., & Simoes, M. G. (2003). A comprehensive review for industrial applicability of artificial neural networks. IEEE transactions on industrial electronics, 50, 585-601.

Merabet, S., Assadi, A. A., Bouzaza, A., & Wolbert, D. (2016). Photocatalytic degradation of indole–4-methylphenol mixture in an aqueous solution: optimization and statistical analysis. Desalination and water treatment, 57, 17039-17050.

Rahman, M. A., Kaneco, S., Suzuki, T., Katsumata, H., & Ohta, K. (2005). Optimized Conditions for the Solar Photocatalytic Degradation of Bisphenol a in Water Using Zinc Oxide. Annali di Chimica, 95, 715-719.

Rosenfeldt, E. J., & Linden, K. G. (2004). Degradation of endocrine disrupting chemicals bisphenol A, ethinyl estradiol, and estradiol during UV photolysis and advanced oxidation processes. Environmental Science & Technology, 38, 5476-5483.

Sabonian, M., & Behnajady, M. A. (2014). Artificial neural network modeling of Cr(VI) photocatalytic reduction with TiO2-P25 nanoparticles using the results obtained from response surface methodology optimization. Desalination and water treatment, 1-11.

Sin, J.-C., Lam, S.-M., Mohamed, A. R., & Lee, K.-T. (2012). Degrading Endocrine Disrupting Chemicals from Wastewater by TiO 2 Photocatalysis: A Review. International Journal of Photoenergy.

Sivanandam, S., Sumathi, S., & Deepa, S. (2006). Introduction to Neural Networks using MATLAB 6.0: Tata McGraw-Hill Education.

Solomatine, D., See, L. M., & Abrahart, R. J. (2008). Data-Driven Modelling: Concepts, Approaches and Experiences. In R. J. Abrahart, L. M. See & D. P. Solomatine (Eds.), Practical Hydroinformatics: Computational Intelligence and Technological Developments in Water Applications (pp. 17-30). Berlin, Heidelberg: Springer Berlin Heidelberg.

Sornalingam, K., McDonagh, A., & Zhou, J. L. (2016). Photodegradation of estrogenic endocrine disrupting steroidal hormones in aqueous systems: Progress and future challenges. Science of the Total Environment, 550, 209-224.

Tanasa, D. E., Piuleac, C. G., Curteanu, S., & Popovici, E. (2013). Photodegradation process of Eosin Y using ZnO/SnO2 nanocomposites as photocatalysts: experimental study and neural network modeling. Journal of Materials Science, 48, 8029-8040.

Tijani, J. O., Fatoba, O. O., & Petrik, L. F. (2013). A review of pharmaceuticals and endocrine-disrupting compounds: sources, effects, removal, and detections. Water, Air, & Soil Pollution, 224, 1-29.

Vaez, M., Omidkhah, M., Alijani, S., Zarringhalam Moghaddam, A., Sadrameli, M., & Gholipour Zanjani, N. (2015). Evaluation of photocatalytic activity of immobilized titania nanoparticles by support vector machine and artificial neural network. The Canadian Journal of Chemical Engineering, 93, 1009-1016.

Viennet, R., Fonteix, C., & Marc, I. (1996). New multicriteria optimization method based on the use of a diploid genetic algorithm: Example of an industrial problem. In European Conference (pp. 120-127): Springer.

Wang, J., Fan, X. M., Tian, K., Zhou, Z. W., & Wang, Y. (2011). Largely improved photocatalytic properties of Ag/tetrapod-like ZnO nanocompounds prepared with different PEG contents. Applied Surface Science, 257, 7763-7770.

Wang, R., Ren, D., Xia, S., Zhang, Y., & Zhao, J. (2009). Photocatalytic degradation of Bisphenol A (BPA) using immobilized TiO 2 and UV illumination in a horizontal circulating bed photocatalytic reactor (HCBPR). Journal of Hazardous materials, 169, 926-932.

Witek-Krowiak, A., Chojnacka, K., Podstawczyk, D., Dawiec, A., & Pokomeda, K. (2014). Application of Response Surface Methodology and Artificial Neural Network methods in modelling and optimization of biosorption process. Bioresource Technology, 160, 150-160.

Xi, J., Xue, Y., Xu, Y., & Shen, Y. (2013). Artificial neural network modeling and optimization of ultrahigh pressure extraction of green tea polyphenols. Food Chemistry, 141, 320-326.

Xie, W., Li, Y., Sun, W., Huang, J., Xie, H., & Zhao, X. (2010). Surface modification of ZnO with Ag improves its photocatalytic efficiency and photostability. Journal of Photochemistry and Photobiology A: Chemistry, 216, 149-155.

Supplementary material

Modeling and Optimization of a photocatalytic process: Degradation of endocrine disruptor compounds by Ag/ZnO

Alma Berenice Jasso-Salcedo[a1], Sandrine Hoppe[b], Fernand Pla[b], Vladimir Alonso Escobar-Barrios[c], Mauricio Camargo[d], Dimitrios Meimaroglou[b]

[a]Instituto Potosino de Investigación Científica y Tecnológica, División Ciencias Ambientales, Camino a la Presa de San José 2055, Col. Lomas 4a Sección. C.P. 78216, San Luis Potosí, S.L.P., México.

[b]CNRS, Laboratoire Réactions et Génie des Procédés, Université de Lorraine UMR 7274, Nancy, F-54001, France.

[c]Instituto Potosino de Investigación Científica y Tecnológica, División Materiales Avanzados, Camino a la Presa de San José 2055, Col. Lomas 4a Sección. C.P. 78216, San Luis Potosí, S.L.P., México.

[d]Université de Lorraine, ERPI, Equipe de Recherche sur les Processus Innovatifs, EA 6737, Nancy, F-54001, France.

[1] Present address author AB Jasso-Salcedo: Department of Materials and Environmental Chemistry, Arrhenius Laboratory, Stockholm University, SE-106 91 Stockholm, Sweden.

Table S1. MSE values corresponding to different network topologies of the developed models

ANN_1 - PD					ANN_1 - IMP				
Topology	**MSE All**	**MSE Train**	**MSE Val**	**MSE Test**	**Topology**	**MSE All**	**MSE Train**	**MSE Val**	**MSE Test**
8:10	5.13E-05	7.42E-05	1.98E-14	1.99E-06	**10:10**	2.40E-03	2.84E-03	2.74E-03	1.22E-04
7:8	5.80E-05	8.11E-05	8.43E-06	6.05E-06	**6:10**	2.41E-03	3.27E-03	9.80E-04	4.02E-05
9:8	8.25E-05	9.69E-05	7.84E-05	2.29E-05	**10:3**	2.42E-03	3.46E-03	2.17E-04	6.83E-05
5:4	1.35E-04	1.28E-04	2.69E-05	2.76E-04	**9:6**	2.49E-03	3.24E-03	1.22E-03	4.11E-04
8:3	1.38E-04	1.42E-04	1.86E-04	7.11E-05	**9:2**	2.52E-03	2.77E-03	1.41E-04	3.79E-03
4:9	1.50E-04	7.27E-05	6.27E-04	1.15E-05	**7:5**	2.63E-03	1.05E-05	2.76E-05	1.67E-02
3:8	1.87E-04	2.22E-04	5.66E-05	1.68E-04	**3:5**	2.66E-03	3.46E-03	8.28E-04	9.82E-04
10:3	1.93E-04	1.71E-04	4.13E-04	7.12E-05	**5:1**	2.70E-03	3.85E-03	2.16E-04	1.12E-04
7:1	1.99E-04	2.57E-04	9.56E-05	4.97E-05	**9:9**	2.71E-03	3.93E-03	1.58E-06	6.00E-05
8:5	2.29E-04	5.57E-05	3.80E-05	1.18E-03	**6:2**	2.74E-03	1.28E-03	1.17E-02	1.82E-04
ANN_2 - PD					ANN_2 - IMP				
Topology	**MSE All**	**MSE Train**	**MSE Val**	**MSE Test**	**Topology**	**MSE All**	**MSE Train**	**MSE Val**	**MSE Test**
9:8	1.56E-04	1.63E-04	1.11E-04	1.68E-04	**8:10**	1.10E-04	1.69E-04	2.79E-11	8.81E-11
17	4.39E-04	5.34E-04	7.90E-06	3.64E-04	**3:10**	1.39E-04	2.15E-04	3.14E-08	1.10E-08
8:8	6.33E-04	7.28E-04	6.62E-04	9.73E-05	**8:4**	1.50E-04	1.23E-04	4.01E-04	1.48E-08
4:9	8.32E-04	4.15E-04	2.48E-03	1.40E-03	**11**	2.06E-04	1.28E-06	2.16E-06	1.16E-03
4:7	1.04E-03	9.44E-04	9.74E-07	2.59E-03	**8:7**	5.45E-04	7.42E-04	6.20E-05	3.05E-04
14	1.18E-03	1.15E-03	7.75E-05	2.46E-03	**9:4**	8.41E-04	6.31E-04	3.32E-19	2.45E-03
15	1.19E-03	1.60E-03	2.83E-07	1.71E-04	**9:10**	1.20E-03	5.95E-05	2.58E-04	6.33E-03
8:10	1.22E-03	1.37E-03	8.44E-04	7.48E-04	**10:1**	1.25E-03	1.80E-03	2.44E-04	2.67E-04
16	1.38E-03	1.76E-03	6.10E-04	9.68E-05	**5:10**	1.33E-03	2.01E-03	1.46E-04	3.38E-05
3:7	1.48E-03	2.01E-03	1.22E-04	5.52E-05	**16**	1.42E-03	2.17E-03	1.49E-05	4.78E-05